Interface Formation between CdS and Alkali Post-Deposition Treated $Cu(In,Ga)Se_2$ Thin Film Solar Cell Absorbers – Key to Understanding the Efficiency Gain?

Penghui Yang,[†] *Regan G. Wilks,*[†,‡] *Wanli Yang,*[§] *and Marcus Bär*[*,†,‡,‖,#]

[†]Dept. Interface Design, Helmholtz-Zentrum Berlin für Materialien und Energie GmbH, 12489 Berlin, Germany.

[‡]Energy Materials In-Situ Laboratory Berlin (EMIL), Helmholtz-Zentrum Berlin für Materialien und Energie GmbH, Berlin, 12489 Berlin, Germany.

[§]Advanced Light Source Lawrence Berkeley National Laboratory, Berkeley, CA 94720, USA

[‖]Department of Chemistry and Pharmacy, Friedrich-Alexander-Universität Erlangen-Nürnberg, Egerlandstr. 3, 91058 Erlangen, Germany

[#]Helmholtz Institute Erlangen-Nürnberg für Renewable Energy (HI ERN), Albert-Einstein-Str. 15, 12489 Berlin, Germany

KEYWORDS: chalcopyrite thin-film solar cell, alkali fluoride post-deposition treatment, $CdS/Cu(In,Ga)Se_2$ interface, chemical structure, x-ray emission spectroscopy, x-ray photoelectron spectroscopy

ABSTRACT: A combination of x-ray photoelectron / Auger electron spectroscopy and soft x-ray emission spectroscopy has been employed to investigate the impact of different alkali post-deposition absorber treatments (PDTs) on the chemical structure of the (buried) CdS/Cu(In,Ga)Se_2 heterojunction; the key interface in chalcopyrite-based thin-film solar cells. Chemical bath deposited (CBD) CdS layers of different thickness on NaF PDT ($CIGSe^{NaF}$) and on NaF+KF PDT ($CIGSe^{NaF+KF}$) Cu(In,Ga)Se_2 absorbers prepared at low temperature (to facilitate the use of flexible, e.g. polyimide, substrates) were studied. While we find the CdS/$CIGSe^{NaF}$ interface to be mainly free of significant chemical interaction, in the proximity of the CdS/$CIGSe^{NaF+KF}$ interface an elemental redistribution involving Cd, In, K, S, and Se is revealed. For the early stages of the CBD-CdS process, our findings are in agreement with the conversion of the K-In-Se type layer present on the $CIGSe^{NaF+KF}$ surface into a mixed Cd-In-(O,OH,S,Se) type layer, probably having some Cd-In and (S,O)-Se composition gradients. For long CBD times – independent of employed PDT – we find the buffer material to be best described by a Cd(O,OH,S) like species rather than being a pure CdS buffer. These findings shed light on the observed performance leap of corresponding CdS/$CIGSe^{NaF+KF}$ – based solar cells.

1. Introduction

Recently, (heavy) alkali fluoride postdeposition treatments (PDTs) led to a boost in power conversion efficiencies for Cu(In,Ga)Se_2 (CIGSe) – based solar cells, now being well above 20%.[1-4] After it was discovered that the incorporation of sodium – which usually diffuses from the commonly used soda-lime glass (SLG) substrate into the absorber during the absorber preparation at elevated temperature – into the CIGSe absorber improved solar cell performance,[5-6] the PDT was developed to deliberately incorporate sodium into CIGSe films deposited on alkali-free

(flexible) substrates.[7] Recently, PDTs have also been used to incorporate other alkalis (heavier than Na) into CIGSe.[1, 3, 8] A combined, sequential NaF+KF PDT of CIGSe absorbers prepared at low temperature (to facilitate the use of flexible, e.g. polyimide, substrates) leads to an improvement of solar cell performance; mainly due to an increase of the short-circuit current.[1] This is explained by the fact that the NaF+KF PDT enables a significant reduction of the CdS layer thickness – the standard buffer layer in CIGSe – based solar cells – without compromising interface quality preventing the commonly observed losses in open-circuit voltage and fill factor.[9] As a consequence, the parasitic absorption in the UV regime due to the CdS is dramatically reduced, benefitting the short-circuit current. Furthermore, a pronounced NaF+KF PDT – induced modification of the CIGSe surface was observed: Several groups report on the presence of K[1-2, 10] accompanied with significant Cu[11-12] and Ga[1] depletion, the formation of a K−In−Se type surface species,[10, 13-15] and a related pronounced band gap widening at the absorber surface. [16-18]. However, only little is known about how this NaF+KF PDT induced absorber surface modification impacts the interface formation between CdS (the standard buffer layer in CIGSe-based solar cells) and the absorber. Reinhard et al. [2] show that the K signal at the surface of a NaF+KF PDTed CIGSe surface is significantly reduced upon rinsing in diluted aqueous ammonia and that the Cd signal after a respective partial electrolyte treatment is significantly higher for NaF+KF PDTed CIGSe surfaces compared to similarly treated CIGSe absorbers that only underwent a NaF PDT or no PDT at all. While the CdS/CIGSe interface were not specifically addressed in that paper, the findings related to the aqueous ammonia rinse and the Cd partial electrolyte treatment could be relevant for the processes dominating the early stages of the CdS chemical bath deposition (CBD) process. Nicoara et al. study the impact of a KF-PDT on the aging of CIGSe surfaces and its interface with CdS,

focusing on very short (1 min) CBD times.[19] Together with Lepetit et al.,[13] they speculate on the formation of an interface layer with a Cd−In−(S,O/OH)$_4$ composition.

Considering the importance of the CdS/CIGSe interface for the device performance, it is crucial to study the interface formation between CdS buffer and CIGSe absorber and how e.g. this is influenced by a KF PDT. This will be important to gain a detailed insight in the underlying mechanism of the apparent beneficial role of performing a KF PDT on the solar cell performance, i.e., enabling a significant reduction of the CdS buffer layer thickness.

Consequently, we studied the structure of the CdS/CIGSe interface and how it is impacted by different alkali PDTs by a combination of different x-ray spectroscopies. The interface formation is investigated by studying sample sets with different CdS thicknesses. We find a pronounced difference between the chemical buffer/absorber interface structures in the case of a NaF or a NaF+KF PDT applied to the CIGSe absorber prior to buffer deposition, providing new insight on the role of potassium in interface formation and its positive impact on device efficiency.

2. Experimental Section

The investigated Cu(In,Ga)Se$_2$ (CIGSe) samples were prepared at EMPA in a low-temperature multistage process according to Ref. [1]. The absorbers were deposited onto a molybdenum coated glass substrate. A silicon oxide diffusion barrier was deliberately put in-between Mo and glass to prevent uncontrollable alkali out-diffusion, mimicking the situation of using alkali-free substrates, as e.g. flexible polyimide. After CIGSe formation a post-deposition treatment (PDT) with NaF (→ CIGSe^{NaF}) or NaF+KF (→ CIGSe^{NaF+KF}) were used to incorporate alkalis into (the upper region of) the absorber in a very controlled fashion (see Ref. [1] for more details). CdS layers were prepared on the CIGSe^{NaF} and CIGSe^{NaF+KF} absorbers by chemical bath deposition (CBD) following the recipe detailed in Ref. [1]. In order to study the buffer/absorber interface formation CdS thickness

series were deposited on the two different absorbers by interrupting the CBD time after 5s, 30s, 1 min, 2 min, 4 min, 15 min, and 24 min for the CdS/CIGSe^{NaF} sample set and after 5s, 30s, 1 min, 2 min, 4 min, 8 min, and 15 min for the CdS/CIGSe^{NaF+KF} sample set. The longest CBD times represent the standard deposition time used for the preparation of solar cell devices based on CIGSe^{NaF} and CIGSe^{NaF+KF} absorbers, respectively. The approximate CdS thicknesses in these cases are 60-70 and 30 nm for the buffer layer deposited on CIGSe^{NaF} (within 24 min CBD time) and on CIGSe^{NaF+KF} (within 15 min CBD time).[1] Corresponding solar cells achieve power conversion efficiencies of round 18 % using a NaF PDT and 20 % using a NaF+KF PDT.[20]

To minimize surface contamination, all samples were packed in a N_2-filled glovebox at EMPA immediately after the CBD-CdS process. At HZB, the samples were unpacked in the N_2-filled glovebox directly connected to the ultra-high vacuum (UHV) surface analysis system. Hence, the CdS/CIGSe samples were transferred the system's load lock chamber without air exposure.

For the characterization by x-ray photoelectron (XPS) and x-ray excited Auger electron (XAES) spectroscopy, we used a non-monochromatized Mg K_α (1253.56 eV) x-ray source and a SPECS PHOIBOS 150 MCD electron energy analyzer. The base pressure in the analysis chambers was $\leq 3 \times 10^{-10}$ mbar. The electron energy analyzer was calibrated according to D. Briggs et al.[21] For the collection of the XPS survey and XPS and XAES detail spectra, the pass energies were 50 and 30 eV, respectively. XPS line intensities were quantified by fitting them with Voigt profiles and a linear background using the curve-fitting and data analysis program Fityk.[22] The probing depth governing inelastic mean free path of the probed electrons ranges between 1 – 3 nm for the used measurement parameters.[23] For more details, also on the analysis of the XAES spectra see Supplemental Information, S.I.

Additional x-ray emission spectroscopy (XES) measurements at the Se $M_{4,5}$ and the S $L_{2,3}$/Se $M_{2,3}$ edges were performed using the Soft X-ray Fluorescence (SXF) spectrometer installed at beamline 8.0.1 of the Advanced Light Source (ALS), Lawrence Berkeley National Laboratory. The base pressure of the SXF analysis chamber was $\leq 1 \times 10^{-9}$ mbar. The energy scales of the XES spectra were calibrated using elastically scattered photons in the range of 100−120 eV in second diffraction order of the spectrometer for the Se $M_{4,5}$ and CdS reference data[24] for the S $L_{2,3}$/Se $M_{2,3}$ energy window. Assuming that the probing depth governing attenuation length in our complex CdS/CIGSe layer structure can be represented by the attenuation length in $CuInSe_2$ (ρ = 5.77 g/cm^3) for the bare CIGSe absorber (and thin buffer) layer(s) and by the attenuation length in CdS (ρ = 4.83 g/cm^3) for the CdS/CIGSe samples with thick buffer layers, the effective attenuation length[25] (that considers both, the attenuation of the photons on their way in and the attenuation of the photons on their way out of the material) is around 15 nm for the Se $M_{4,5}$ and ranges between 20 and 60 nm for the S $L_{2,3}$ XES measurements and the used experimental setup. For more details see S.I.

For transport to the ALS, the samples were sealed under N_2-atmosphere. However, during introduction into the SXF UHV chamber, the samples were shortly (< 5 min) exposed to ambient air.

3. Results and Discussion

To study the impact of a NaF+KF PDT on the chemical structure of the CdS/CIGSe interface, a thickness series of CdS was prepared by CBD (CdS/CIGSe^{NaF+KF}) and studied by XPS, XAES, and XES. In order to isolate the effect of potassium, the CdS/CIGSe^{NaF+KF} data is compared to the measurements of corresponding CdS/CIGSe samples for which the absorber was only subject to a NaF PDT (CIGSe^{NaF}). The XPS survey spectra of the two CdS/CIGSe sample series are shown in

S.I., Figure S1. As expected, all Cu, In, Ga, Se, Cd, and S photoemission and Auger lines are present. The Cu, In, Ga, and Se peaks decrease in intensity, and Cd and S peaks increase with increasing CBD time, as expected. A Na-related XPS signal (most prominently the Na 1s line at 1071 eV binding energy) can only be observed for CdS/CIGSe^{NaF} samples. The apparent KF PDT – induced disappearance of Na from the absorber was observed before[2] and an ion exchange mechanism was proposed as explanation.[26] In addition, the presence of substantial C- and O-related XPS and XAES signals suggest surface contamination and/or incorporation of C and O into the deposited absorber and buffer layers (as discussed below). The Cu signal intensity of the bare CIGSe^{NaF+KF} is significantly lower than for the CIGSe^{NaF} absorber, consistent with a strong surface Cu depletion, as previously reported.[1-2, 27]

For more detailed chemical and electronic structure information, higher-resolution detail spectra were measured and are displayed – along with curve fitting results – in S.I., Figures S2-S11. To derive the absorber surface composition, we have used the shallow core level lines of the absorber elements (Cu 3p, Se 3d, In 4d, Ga 3d; neither alkali elements nor C and O are included in this analysis). Due to the very similar kinetic energy of the related photoelectrons, we are able to neglect the variations in electron analyzer transmission function and inelastic mean free path (IMFP) on signal intensity and hence only correct for the different photoionization cross sections [28] for quantification. The surface Cu:(In+Ga):Se compositions are ≈ 1.0:2.8:3.9 and ≈ 1.0:6.8:9.8 for the bare CIGSe^{NaF} and CIGSe^{NaF+KF} absorbers, respectively; we find a different degree of surface Cu-deficiency, in agreement with Refs.[1-2, 10, 27, 29]. As in our previous report, we attribute the heavier Cu depletion of the CIGSe^{NaF+KF} absorbers to the formation of a K-In-Se type species on top of the CIGSe absorber.[10] The Ga/(Ga+In) (GGI) ratio is derived to be (0.22 ± 0.05) and (0.04 ± 0.05) for CIGSe^{NaF} and CIGSe^{NaF+KF}, respectively. This confirms previous XPS studies of

the impact of KF PDTs on the chemical CIGSe surface structure,[1, 10] suggesting that employing a NaF+KF PDT leads not only to a strong Cu-depletion but also Ga-depletion near the absorber surface.

Next, we discuss the chemical structure at the CdS/CIGSe interface and how it is influenced by the different PDTs. To do so, we consider the effective CdS thickness values calculated from the attenuation of each absorber (shallow) core level line (and from the increasing intensity of the Cd and S lines); these element-specific thicknesses are displayed as functions of CBD time in Figure 1. More details on the calculation are given in S.I.

The effective element-specific thicknesses derived for the CdS/CIGSe^{NaF} samples increase with CBD time and agree for all elements within the error bar as shown in Figure 1a. Note that the thickness plateau above 4 min CBD time is caused by the saturation of the Cd 3d and S 2s signal (i.e., after 4 min CBD, the layer is "infinitely" thick compared to the XPS information depth) and thus does not accurately represent the true CdS thickness but rather shows the limitation of this approach. The Na-related effective thickness agrees for CBD times up to 1 – 2 min, but indicates a significantly lower thickness value for a CBD time of 4 min. This can be explained by redeposition (from the chemical bath) or diffusion (from the CIGSe^{NaF} absorber). Based on this preliminary examination of the effective thickness calculations, it appears that the buffer layer grows without strong interfacial interaction between absorber and buffer elements. This is in contrast to our previous reports[30] in which we see a S/Se intermixing at the CdS/CIGSe interface, but could be explained by a different absorber surface structure formed during the low-temperature deposition process (compared to the absorbers from a high-temperature deposition process studied in the past). It is important to note that the CIGSe^{NaF} deposition process was not optimized to produce the best-performing cells, rather it was as similar as possible to the CIGSe^{NaF+KF} process;

the absorber surface structure of an optimized $CIGSe^{NaF}$ may differ in a significant enough way that S/Se intermixing could occur.

The effective element-specific thicknesses derived for the $CdS/CIGSe^{NaF+KF}$ samples are shown in Figure 1b. The direct comparison with the thickness values derived for the $CdS/CIGSe^{NaF}$ samples shows clear differences. After a 5 s CBD, all the derived thicknesses except for the Se-extracted values have increased, with the largest thicknesses (exceeding that derived for the $CdS/CIGSe^{NaF}$ samples) determined for Cu and K, i.e., the intensity of the Cu 3p and K 2p lines have decreased most. From 5 s to 30 s CBD time, the thickness values based on the intensity evolution of the absorber elements (including K) then decrease to an extent to even result in "negative thicknesses" for In, Ga, K, and Se. Note that the drop is biggest for K and very similar for all other absorber elements. These "negative values" reflect the increase of the respective XPS line intensities to values above those measured for the bare $CIGSe^{NaF+KF}$ absorber, indicating significant chemical interaction involving these elements during that CBD period. For CBD times of 1 min and longer all thickness values increase steadily (with some variation for K-based values – indicating a more complex situation, as discussed below) as it would be expected for regular buffer layer growth. Furthermore, we observe a different behavior for the Cd and S derived thickness values. Especially for CBD times below 2 min, the Cd-based thicknesses are significantly larger than the S-based thicknesses and the corresponding thickness in the $CdS/CIGSe^{NaF}$ series. This difference indicates that at early stages of CdS CBD on $CIGSe^{NaF+KF}$, Cd is deposited not (only) as stoichiometric CdS but might be incorporated into the upper surface of the $CIGSe^{NaF+KF}$ absorber and/or present in other chemical forms.

In order to get insight into the chemical nature of this potentially modified absorber region, we performed complementary Se $M_{4,5}$ XES measurements. The background normalized Se $M_{4,5}$ XES

spectra of the CdS/CIGSe^{NaF} and CdS/CIGSe^{NaF+KF} sample sets are shown in Figure 2. The spectra are produced through relaxation of a Se 3d core-ionized excited state; in a simple picture a (4p-like) valence electron decays into the 3d core hole, leading to emission of a photon. The energy-resolved spectrum of the measured photons is therefore related to the Se projected density of occupied states. The spectra of the bare CIGSe absorbers are similar to what was previously observed for similarly prepared samples.[10] For the CIGSe^{NaF} series, the CBD process leads only to a decreased intensity of the XES signals without a change in spectral shape (confirmed by area normalized spectra in S.I., Figure S16a suggesting the Se chemical environment is dominated by the absorber. For the CdS/CIGSe^{NaF+KF} series, there is a drop in intensity and clear change in spectral shape in the CBD treated samples compared to the bare absorber, with the shape of all CBD treated samples remaining the same**,** corroborated by the area-normalized spectra in S.I., Figure S16b. The spectral difference in the Se $M_{4,5}$ spectra of the CIGSe^{NaF} and the CIGSe^{NaF+KF} absorber is consistent with our previous observations[10] and can be explained by formation of a K-In-Se layer in the latter case. The CBD-induced changes in the CIGSe^{NaF+KF} series spectra suggest that this layer is modified due to buffer deposition; the CdS/CIGSe^{NaF+KF} spectra do not however simply resemble those of the CIGSe^{NaF} series, suggesting that a significant quantity of a different Se-containing material is formed in the former case. To identify the new Se compound, we attempt to reconstruct the measured CdS/CIGSe^{NaF+KF} spectra with a superposition of reference spectra of CIGSe^{NaF}, KF-In_2Se_3 (considered as being representative for the chemical structure of a K-In-Se type species), and CdSe in S.I., Figure S17. Note that all the spectra (including reference spectra) used for fitting are area normalized. As previously published[10] and discussed above, the CIGSe^{NaF+KF} spectrum can be modelled as a sum of the spectra of CIGSe^{NaF} and of a KF-treated In_2Se_3 sample with the relative contributions falling between those derived from the previously

published alkali-poor and alkali-rich spectra.[15] The spectra of the CdS/CIGSe^{NaF+KF} series can be presented as a sum of the spectra of the bare CIGSe^{NaF} and a CdSe reference (see S.I., Figure S17). However, due to the broadness of the spectra, other fit models can also be successfully applied: an equally good fit can be obtained from a sum of bare CIGSe^{NaF+KF} and CdSe reference spectra (see S.I., Figure S18). In the CIGSe^{NaF} + CdSe model, the relative contribution of the CdSe to the fit is larger than in the CIGSe^{NaF+KF} + CdSe model. In conclusion, based on this analysis we cannot distinguish whether the K-In-Se type species is present at the CdS/CIGSe^{NaF+KF} interface or whether it is dissolved/modified (partially or completely) in the chemical bath.

However, based on the discussion in S.I. around Figure S19, it appears that the majority of K that is present at the surface of the CIGSe^{NaF+KF} absorber is dissolved in the CBD (in agreement with Ref. [2], and re-deposited as K-O type species. In that case, the K-In-Se compound would no longer be present, and so of the two Se $M_{4,5}$ XES fit models described above, we would favor the CIGSe^{NaF} + CdSe model for representing the CdS/CIGSe^{NaF+KF} data. This would mean that in the first stage of the CBD-CdS process the K-In-Se type compound is (partially) dissolved and replaced by a species containing Cd-Se bonds. Note that the identification of K-O bonds might be an artefact of sample preparation (i.e., CBD break off after short times with subsequent sample rinsing). This ‘conversion’ of the K-In-Se into a Cd-Se bond containing species could be promoted by amine-complexes present in the CBD solution (see Refs.[31-32] for examples of corresponding interface interactions). Based on different stability constants different ion-exchange processes during the induction period of the chemical bath process could take place resulting in the observed modification of the chemical structure.

To clarify and expand on the findings based on the Se $M_{4,5}$ XES data, we use the In and Cd 3d XPS and $M_4N_{45}N_{45}$ (MNN) XAES as further sensitive probe of chemical structure. The proximity

and overlap of the XAES spectra require a careful process to separate them; this is described in S.I. in conjunction to Figure S20. Each measured In $3d_{3/2}$ spectrum can be fitted by a single Voigt function, all with the same Gaussian and Lorentzian contributions (see S.I., Figure S9). For the CdS/CIGSe^{NaF} series, there is a shift of ~0.2 eV to higher binding energies for the samples with CdS compared to the bare absorber; this same shift is also seen in the other absorber cation (i.e., Cu, In, Ga) related core levels of this series (see S.I., Figures S8-S10). The In $3d_{3/2}$ binding energy of the CIGSe^{NaF+KF} is <0.1 eV lower than that of the CIGSe^{NaF}, and the changes in the CdS/CIGSe^{NaF+KF} series are more complex – despite still being modelled with a single Voigt – with a shift of ~0.15 eV to lower binding energy after 30s CBD. This shift is not reproduced in the other absorber cations core levels spectra of this series (see S.I., Figures S8-S10); the Cu and Ga 2p of the CdS/CIGSe^{NaF+KF} series rather undergo a similar shift (~0.2 eV to higher binding energy after CdS deposition) to what is seen in the CdS/CIGSe^{NaF} series.

The spectral shape of the In MNN of the CdS/CIGSe^{NaF} samples is largely independent of CdS deposition (see Figure 3a), in agreement with the single Voigt function fit of the In $3d_{3/2}$ (S.I., Figure S9). Thus, for this series, all In MNN spectra can be represented by the sum of the (scaled and shifted) In MNN spectrum of the bare CIGSe^{NaF} absorber (component In_a) and a suitable (Cd MNN induced) background spectrum (i.e., the spectrum of the 24 min – CdS/CIGSe^{NaF} sample). However, the In MNN spectra of the CdS/CIGSe^{NaF+KF} series do change in spectral shape upon CdS deposition and with CdS deposition time (see Figure 3b). In order to analyze these spectra, we use the In MNN spectrum of the bare CIGSe^{NaF} absorber (which has the narrowest shape and thus is used as a reference spectrum representing a single In species) to fit the In MNN spectra of the CdS/CIGSe^{NaF+KF} sample set. In this procedure, each spectrum can be reproduced as a sum of two contributions (plus 15 min – CdS/CIGSe^{NaF+KF} background spectrum) – one at almost constant

energy position corresponding to the CIGSe^{NaF} In_a position (and thus also attributed to species In_a) and a second species which shifts as a function of CBD time, attributed to In_b, In_c, and In_d. In order to identify these components, we next consult the modified Auger parameter.[33-34]

The modified Auger parameter (α′) combines the core level and Auger line related information in a way that cancels variations in sample charging, doping, and surface band bending, allowing chemical species information to be reliably extracted. α′ and its corresponding binding energy and kinetic energy components can be displayed together in a Wagner plot[35] (Figure 4), where the diagonal lines correspond to constant values of α′; all points along a common α′ line are assumed to represent the same chemical species. Hence, for the CdS/CIGSe^{NaF+KF} series, the shifted contributions to the XAES spectra (components In_a – In_d) are treated as distinct chemical species, because the lack of a shift in the corresponding In $3d_{3/2}$ spectra gives them a distinct value of α′. The direct comparison with α′ values for related In-compounds ($CuInSe_2$, $CuIn_3Se_5$, In_2Se_3, In_2S_3, In_2O_3 and a KF-treated In_2Se_3 – considered to represent the chemical structure of a K-In-Se – type species;[10] see S.I. for more details on how the reference boxes have been defined) reveals that the modified Auger parameter for component In_a is attributed to a similar chalcopyrite type environment for both CdS/CIGSe sample series. Note that the α′ value for the CdS/CIGSe^{NaF} samples lie on the same diagonal as the values of the bare absorbers, although the binding energy value falls slightly outside the reference box defined by published binding energies. The modified Auger parameter of component In_b, which is only found for the bare CIGSe^{NaF+KF} absorber, agrees – within experimental uncertainty – with that of the K-In-Se – type species, confirming our earlier study[10] and agreeing with our Se $M_{4,5}$ XES finding above. For the 5s and 30s CdS/CIGSe^{NaF+KF} the In_c species appear in the Auger spectra, while the core level spectra remain at the same binding energy as the bare absorber. The α′ value of In_c suggests the formation of an In-containing interface

species (which is most likely related to the above discussed 'conversion' of the K-In-Se into a Cd-Se bond containing species) in this CBD time regime. Note that the relative contributions of In_a and In_c are nearly constant for the two spectra. Component In_d is found for 1, 2, 4 min $CdS/CIGSe^{NaF+KF}$ samples and can clearly be attributed to the formation of In-O bonds. After 1 min CBD time, the chemical environment of In ceases to change, and there is only a decrease in the corresponding XPS/XAES intensities caused by attenuation of the signal by the growing buffer layer. The fact that the Se $M_{4,5}$ XES does not show significant spectral shape changes for CBD times > 5 s, is in agreement with the formation of an In- *and* Se-containing interface species and an additional Se-free In species for CBD times ≥ 1 min. There is a slight discrepancy in the comparison, because as stated above (and shown in Figure 3) it would appear that the interface species In_b disappears after 30s CBD time to be replaced by In_c. However, the fit method applied to the In MNN was to use the minimum possible number of distinct components, and so the fit would be improved by including three components – $In_{a,b,c}$ – in the fits for CBD of more than one minute. The uncertainty in the model means that it is not in contradiction with the Se $M_{4,5}$ results, even more so considering that the Se $M_{4,5}$ spectrum of In_2Se_3 [10] is very similar to that of CdSe (see S.I., Figures S17 and S18). Thus, the spectral Se $M_{4,5}$ fingerprint of In-Se bonds could already be accounted for in the $CIGSe^{NaF}$ + CdSe fit model shown in S.I., Figure S17.

To study the interface formation from the viewpoint of the deposited buffer layer, the Cd modified Auger parameters α' (calculated in similar fashion to the In parameters above) are discussed next. The details of how the Auger spectra were fit and how the overlapping contributions from In MNN are considered are discussed in supporting information (see S.I., Figures S20 and S21, and related discussion). For both $CdS/CIGSe^{NaF}$ and $CdS/CIGSe^{NaF+KF}$ series, two distinct components defined initially as Cd_a and Cd_b, are needed to explain the spectra, but the relative quantities vary

distinctly between the two series (S.I., Figure S22), confirming that the buffer deposition proceeds quite differently depending on PDT. For the CdS/CIGSe^{NaF+KF} series, a strong Cd_a signal forms in the first stage of CBD (i.e., for the 5 s sample). In the discussion of Figure 1b, we described how Cd was deposited without corresponding quantities of S in the early stages of CBD, and when this is coupled with the observed modification in Se $M_{4,5}$ XES (Figure 2b) of the same samples, it strongly indicates that Cd-Se bonds are formed at the interface. This is corroborated by the α' values for Cd_a in Figure 5b, which are directly compared to α' values for related Cd-compounds (CdSe, CdS, CdO, and $Cd(OH)_2$– see S.I. for more details on how the reference boxes have been defined).[34, 36-45] Within the experimental uncertainty, we find an agreement between the modified Auger parameter of CdSe and that of Cd_a (at least for CBD times up to 2 min). However, the fact that due to a seemingly high E_K of the respective Cd MNN spectra, the Cd_a α' values are located outside the indicated CdSe box (i.e., being more in agreement with what would be expected for Cd-O bonds, in particular for the 4 min CdS/CIGSe^{NaF+KF} sample) indicating that the interface compound has a more complex chemical (gradient?) structure than pure CdSe. For larger CBD times, a second species, Cd_b, is present, and the relative Cd_a contribution decreases in a way that is consistent with what would be seen from an interface species, i.e. the Cd_a signal appears to be attenuated by a capping (buffer) layer of increasing thickness. After 8 min CBD, the Cd_a contribution is effectively zero, and the spectra again represent a single phase, Cd_b, representing the completed buffer layer. Based on the comparison and agreement of the α' values for Cd_b with that of CdS, we attribute it to be indicative for Cd-S bonds. (However, note that the composition of the buffer layer is more complex than pure CdS, as will be discussed below.)

For the CdS/CIGSe^{NaF} series, we find the Cd MNN Auger spectrum of the 5s CBD CdS/CIGSe^{NaF} sample in Figure 5a is more complex than the corresponding CdS/CIGSe^{NaF+KF} spectrum, as it

already requires two contributions for an adequate description. We again label these components Cd_a and Cd_b, and their general behavior is similar to that of the corresponding components in the CdS/CIGSe^{NaF+KF} described above, with some difference in specifics. In the CdS/CIGSe^{NaF} series, Cd_a is only a relatively small contributor and disappears completely after 2 min CBD, and again it appears consistent with a species formed at the interface. (Since Cd_a seems to form exclusively in the induction period of the CdS CBD process, it might very well be possible that Cd_a forms only in the early stages of CBD and would no longer be present if the process was not interrupted; i.e., it may be an artifact of the non-standard CBD process used to produce the "thin" buffer layers for this experiment.). The values of α', coupled with the higher Cd 3d binding energies, indicate that in this series Cd_a is likely a CdO species, unlike the corresponding species formed at the CdS/CIGSe^{NaF+KF} interface, as depicted in Figure 5b. Based on the lack of changes in the Se $M_{4,5}$ spectra of the CdS/CIGSe^{NaF}, no significant amount of Cd-Se bonds are expected to be formed for this series. When Cd_b is formed, it is much more uniform in Cd 3d binding energy and α' than the corresponding data in Figure 5b, and falls very close to expected values for CdS. The presence of Cd_b in all spectra, including for very short CBD times, is in agreement with the discussion of Figure 1a. The analysis of the Cd Auger parameter does not suggest that $Cd(OH)_2$ is present in significant amounts in either of the sample sets, however, the respective O 1s spectra in S.I., Figure S11, does show a high binding energy component (O_b) at approx. 532.7 eV, which we attribute to hydroxyl groups. The ratio of O_a (the main O 1s peak in Figure S11, attributed to oxides) to O_b indicates that the amount of hydroxide present is small relative to the oxide content ([12 ± 2]% for the 2 – 24 min CdS/CIGSe^{NaF} samples and [25 ± 3]% for the 2 – 15 min CdS/CIGSe^{NaF+KF} samples). The hydroxide and its corresponding spectral signature (if present) is expected to appear in the measurement of all samples, including the "single species" reference curve used to fit the

Cd MNN curves in S.I., Figure S21. Thus, as long as the hydroxide content is relatively stable, the here performed Auger spectra analysis method is not sensitive to $Cd(OH)_2$, explaining why no $Cd(OH)_2$ species is specifically identified.

The Cd/S ratio (derived from the Cd 3d and S 2s spectra in S.I., Figures S6 and S7) clearly deviates from the stoichiometry expected for CdS independent of performed PDT, as shown in S.I., Figure S23a. For short CBD times, the ratio is quite large, and we attribute this to the formation of S-free (or poor) Cd species at the interface (as indicated in Figure 5 and related discussion). However, even for long CBD times, we find Cd/S ratios of approximately 2 for both sample sets, indicating that the buffer material is not stoichiometric CdS. When the $Cd/(S+O_{a+b})$ ratio is calculated instead, the expected cation:anion ratio of approximately 1:1 is derived for CBD times > 2 min, suggesting that the buffer is better described as a Cd(O,S) like compound. The S 2s (S.I., Figure S7) indicate that the mixed phase is formed without the presence of S-O (i.e., sulfate) bonds, which would be indicated by a clear peak at high binding energy as reported for S 2p.[46] For short CBD times, the $Cd/(S+O_{a+b})$ is still quite large for the $CdS/CIGSe^{NaF+KF}$ sample set, as was the Cd/S ratio, in agreement with the formation of additional Cd-Se bonds at the interface as discussed in conjunction with Figures 2 and 5. For the $CdS/CIGSe^{NaF}$ series, the $Cd/(S+O_{a+b})$ ratio is below 1 for CBD times shorter than 2 minutes, indicating that the (hydr)oxide features O_{a+b} in the O 1s spectra are not exclusively related to Cd.

To further characterize the chemical structure at the buried CdS/CIGSe interface and how it changes with different PDT, S $L_{2,3}$/Se $M_{2,3}$ XES were measured (see Figure 6). The broadness and low cross-section of the Se $M_{2,3}$ make it less useful than the Se $M_{4,5}$ as an indicator of chemical structure, but the S $L_{2,3}$ has been shown to be extremely sensitive to the valence band and chemical structure.[47-48] As in the overlapping XPS spectra in S.I., Figure S7, the S signal intensity increases

while the Se signal is attenuated as CdS thickness increases, as expected. The relative intensities of the S and Se related signals are influenced by a number of factors including fluorescence yield,[49] ionization cross section, depth dependence, etc., and so the specific S/Se signal ratios in XPS and XES will be quite different for the same sample.

For the $CIGSe^{NaF}$ and $CIGSe^{NaF+KF}$ absorbers, the dominant emission feature is attributed to the Se $M_{2,3}$ emission. The energy difference between the main peak and high-emission energy shoulder is 5.7 eV, corresponding to the Se 3p doublet separation.[50] Independent of employed PDT, the S $L_{2,3}$ spectra of samples with long CBD times closely resemble the CdS reference spectrum, which has been reported many times previously,[32, 51] as expected based on the XPS and XAES data described above. The S $L_{2,3}$ spectrum of CdS is composed of emission caused by S 3s→2p transitions, Cd 4d→S 2p transitions, and Cd 5s→S 2p transition from the upper valence band (UVB).[52] For ease of comparison all spectra were multiplied by appropriate scaling factors to be presented with similar intensity. While spectra are essentially identical to the CdS reference spectra for CBD times longer than 4 min, the samples with thinner (30s - 2 min CBD time) CdS overlayers are quite different. Most prominently the emission from Cd 4d→S 2p transitions seems to be almost entirely absent in the spectra of both the CdS/ $CIGSe^{NaF}$ and the CdS/$CIGSe^{NaF+KF}$ sample sets. In the past, this has been interpreted as indication that sulfur is deposited without forming S-Cd bonds[51, 53] or that the CdS deposited during the early stages of the CBD process has a poorly defined physical structure (i.e., different bond lengths and angles), which would result in a broadening of the Cd 4d→S 2p emission features to an extent where they disappear in the noise floor of the measurement.[32] Considering the direct comparison of the S $L_{2,3}$ data of the CdS/CIGSe sample set from Ref. [51] (that indicates the deposition of sulfur without the formation of S-Cd bonds) with our data (see S.I., Figure S24 and connected discussion), the latter explanation, i.e.

the very thin films containing S-Cd bonds formed during short CBD times are poorly defined, seems more likely. This is also in agreement with the finding that in the beginning of the CBD process most of the deposited Cd is not bonded to sulfur (see discussion in S.I., in conjunction with Figure S24). However, the related finding that the buffer layer contains a significant amount of oxygen (see S.I., Figure S23b), does not lead to the formation of sulfates as the distinct spectral signature of -SO_4^{2-} bonds[54] is not observed in any S $L_{2,3}$ spectra, in agreement with the XPS and XAES data.

In order to study the impact of the different PDTs on the chemical interface structure, i.e. aiming at determining whether or not the chemical species formed at the CdS/CIGSe interfaces (e.g., species In_c in Figure 3b and 4 as well as species Cd_a in Figure 5) contain S, the S $L_{2,3}$ XES spectra of the CdS/ $CIGSe^{NaF}$ and the CdS/$CIGSe^{NaF+KF}$ samples for short CBD times are inspected. To do so, the 30 s and 4 min spectra (normalized to same height) from Figure 6 are directly compared in Figure 7. The spectra of the 4 min CdS/CIGSe samples with different PDT are dominated by the spectral signature of CdS, and the spectra do not differ significantly between series. However, for the 30s sample, there are small differences between the $CIGSe^{NaF}$ and $CIGSe^{NaF+KF}$ series. Most prominent is the redistribution of spectral intensity at the maximum of the spectra to higher emission energies when comparing the normalized spectrum of the 30s CdS/$CIGSe^{NaF+KF}$ sample with that of the 30s CdS/$CIGSe^{NaF}$ sample. We attribute this to the spectrum of the 30s CdS/$CIGSe^{NaF}$ sample being dominated by the Se $M_{2,3}$ emission of the CIGSe absorber, while the spectrum of the 30s CdS/$CIGSe^{NaF+KF}$ sample shows a higher contribution of a CdS signature, in agreement with the discussion in conjunction with Figure 1. Reasonable difference spectra can be computed using Se $M_{2,3}$ contributions of up to 30% (see Figure 7). The comparison with the S $L_{2,3}$ spectrum of a In_2S_3 reference spectrum[55] (shifted by -0.7 eV to align with the low-energy slope of

the difference spectrum) indicates the presence of additional spectral intensity between 151 and 153 eV, i.e. the region which is dominated by Cd 4d→S 2p emission features. Considering a model "$CdIn_2S_4$" reference spectrum, which is constructed by adding 0.5 × S $L_{2,3}$ (CdS) and 0.5 × S $L_{2,3}$ (In_2S_3), we find a good agreement with the difference spectrum. The clearly identifiable Cd 4d→S 2p emission features in the "$CdIn_2S_4$" reference spectrum and their absence in the (noisier) difference spectrum is again be attributed to a poorly defined physical structure. Thus, we find indications for the formation of S-Cd *and* S-In bonds at the interface of the CdS/CIGSe^{NaF+KF} but not at the CdS/CIGSe^{NaF} interface (or at least in smaller quantities). Based on our analysis of the In and Cd XPS and XAES data, we relate this Cd-In-S containing interface compound to species In_c (see Figure 3b and 4) and to some extent to species Cd_a (see Figure 5). Note that the position of the related α' (In) between that of In_2S_3 and In_2O_3 (see Figure 4) indicates that also oxygen is incorporated in this compound.

Considering the XPS, XAES, and XES results together, it is possible to make some clear statements about the structure at the CdS/CIGSe^{NaF} interface. When the interface is formed, Cd and S are both present for even the shortest CBD times (Figure 1a), Cd-S and Cd-O bonds (Figure 4 and 6) are formed in the early stages of CBD (Figure 4), the Se chemical environment does not change (Se $M_{4,5}$ XES, Figure 2a), the In chemical environment does not change (Figure 3 a and Figure 4), and for long CBD times the buffer grows as a Cd(O,OH,S)-like compound (Figure 5a, S6, and S21).

The CdS/CIGSe^{NaF+KF} interface structure is more complex, and the interpretation of the results is more ambiguous. When the interface is formed, Cd is initially present in much larger quantities than is S for the shortest CBD times (Figure 1b), the Se chemical environment changes immediately upon CBD but appears stable thereafter (Se $M_{4,5}$ XES, Figure 2b) indicating the

formation of Cd-Se bonds at the interface. In is initially (i.e. for the bare $CIGSe^{NaF+KF}$ absorber) found in two distinct chemical environments (assumed to be of Cu-In-Se and K-In-Se type). Upon CBD a change of the chemical environment of In throughout the first minute of CBD (Figure 3b and Figure 4) can be observed, attributed to the formation of among others In-O bonds for CBD times of 1, 2, and 4 min. The deposited Cd is initially (i.e., for the 5 s sample) a single species which might be best described by a CdSe-like species. Between 30s and 4 min, two Cd species can be identified; one which gradually transforms from CdSe-like to CdO-like and the other one being representative for the thick Cd(O,OH,S)-like buffer compound (Figures 5b, S6 and S21). From the perspective of the sulfur, there is some evidence of the formation of S-In (in addition to formed S-Cd) bonds at the interface (Figure 6). In summary, the first stages (5s, 30s) of interface formation may be dominated by the growth of a Cd-In-(O,OH,S,Se) species with probably some Cd-In and (S,O)-Se composition gradient resulting in an In- and Se- rich composition close to the absorber, possibly formed due to modification/conversion of the existing K-In-Se layer and a Cd- and S,O-rich composition away from the absorber. Note that the while no specific spectral fingerprint-like evidence was presented, from the discussion in conjunction with Figure 1, it cannot be excluded that Ga is also present in this layer. For longer CBD times the growth of a Cd(O,OH,S)-like buffer material prevails. The identified Cd-In-(O,OH,S,Se) species corroborates the reports by Nicoara et al.[19] and Lepetit [13] who speculate that a Cd-In-(S,Se,O/OH) may form. Note that the identification of Cd-O bonds in the early stages (i.e., in the induction period) of the CBD process might, for both sample sets, be an artefact of sample preparation (i.e., CBD break off after short times with subsequent sample rinsing).

The suggested conversion of the K-In-Se type compound formed on top of the $CIGSe^{NaF+KF}$ absorber into a graded Cd-In-(O,OH,S,Se) mixed layer during the initial phase of the CBD-CdS

process, presumably due to amine-complex promoted ion-exchange processes during the induction period of the chemical bath deposition, may be the key to understanding the ability to reduce the CBD time and increase buffer transparency in corresponding solar cell devices without compromising interface quality, preventing losses in open-circuit voltage. The resulting more transparent buffer layer leads to a significant reduction of parasitic absorption, improving the short-circuit current,[1] which is one of the main beneficial effects of employing a heavy alkali PDT.

Furthermore, based on the findings reported in Ref.[17] there are large offsets in the valence and conduction band at the interface between the suggested NaF/KF-PDT – induced K-In-Se – type surface species and the CIGSe absorber, which may limit charge carrier (here in particular electron) transport. Thus, the chemical modification of the K-In-Se – type species into a graded Cd-In-(O,OH,S,Se) interface compound during the early stages of the CdS CBD process may also be beneficial from the electronic interface structure point of view. However, additional measurements specifically addressing this issue are required to conclusively answer this question.

Nevertheless, the gained detailed understanding paves the way to deliberately facilitate the generation of a surface structure that enables the in-situ formation of a high-quality interface during the induction period of a chemical bath process and fully exploit it as novel approach of forming high-quality interfaces in solar cells and other energy conversion devices.

4. Conclusion

X-ray photoelectron spectroscopy (XPS), x-ray excited Auger electron spectroscopy (XAES), and soft x-ray emission spectroscopy (XES) were used to investigate the impact of different alkali post-deposition treatments (PDTs) on the chemical structure of the CdS/CIGSe interface. In order to identify the role of potassium in interface formation, the results on buffer/absorber samples sets have been compared that underwent a NaF or a NaF+KF PDT prior CdS deposition. For both

sample sets we find – independent of PDT – the buffer layer to be best described by a Cd(O,OH,S) compound rather than to be a pure CdS buffer. However, while the buffer/CIGSe^{NaF} structure is formed without major interfacial interaction, significant elemental redistribution involving Cd, In, K, S, and Se in the proximity of the buffer/CIGSe^{NaF+KF} heterojunction is revealed. In detail, we suggest that a mixed Cd-In-(O,OH,S,Se) type layer, with probably some Cd-In and (S,O)-Se composition gradients, is formed in the early stages of the CBD-CdS process presumably due to an ion-exchange promoted modification/conversion of the K-In-Se layer initially present on the CIGSe^{NaF+KF} surface. This interface layer enables the employment of thinner CdS buffer layers and thus the reduction of parasitic absorption while maintaining a high-quality interface. It is (one) key to understand the beneficial impact of the NaF+KF PDT on corresponding solar cells and opens the route for deliberate device optimization.

FIGURES

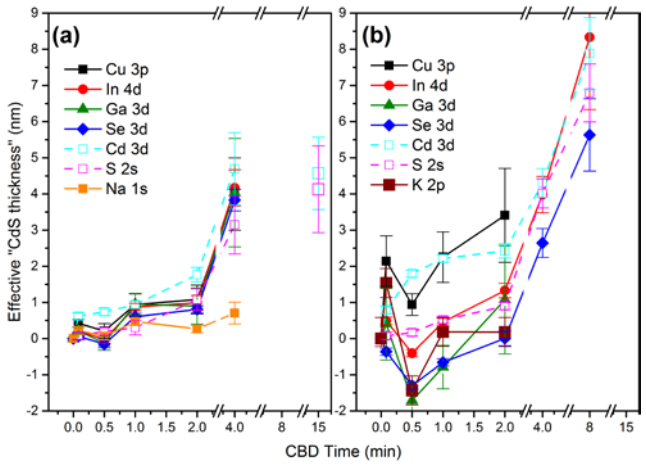

Figure 1. Evolution of the effective "CdS" layer thicknesses for the CdS/CIGSe^{NaF} (a) and CdS/CIGSe^{NaF+KF} (b) samples with increasing CBD time. The thickness values have been calculated based on the fit results in S.I., Figures S2-S11, and the respective inelastic mean free path (IMFP, calculated by TPP2M[23] – more details can be found in S.I.).

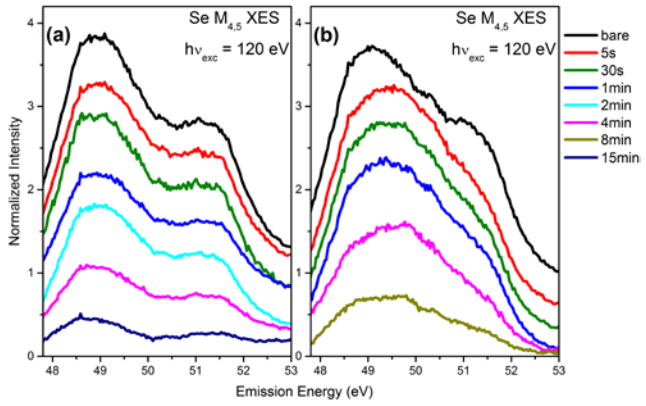

Figure 2. Background normalized Se $M_{4,5}$ XES spectra of the CdS/CIGSe^{NaF} (a) and CdS/CIGSe^{NaF+KF} (b) sample series. For clarity, a vertical offset was added.

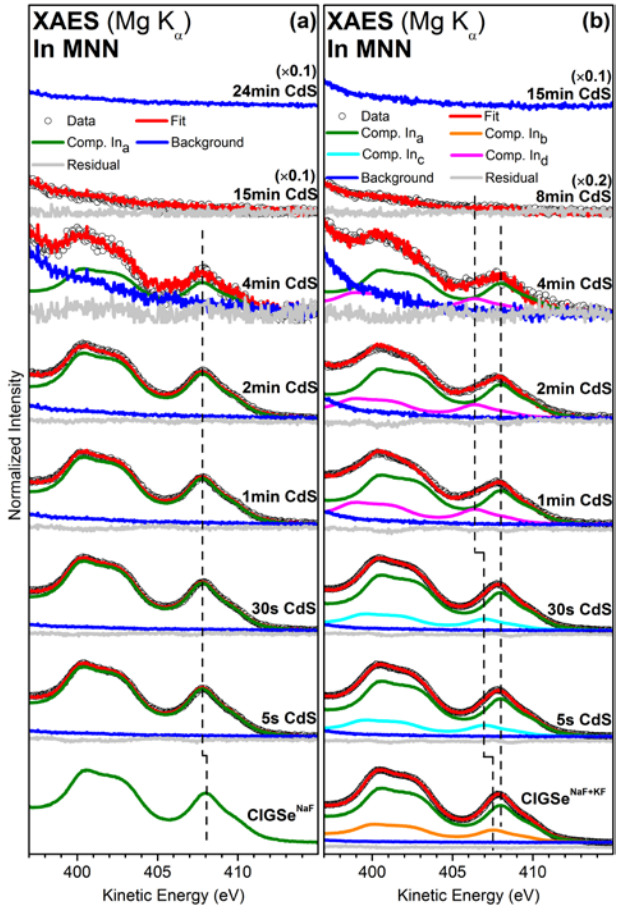

Figure 3. In $M_{45}N_{45}N_{45}$ XAES spectra of the CdS/CIGSe^{NaF} (a) and CdS/CIGSe^{NaF+KF} (b) sample series together with their spectral analysis. The reference spectra summed up to represent the data are the (scaled and shifted) In MNN spectra of bare CIGSe^{NaF} absorber and a suitable (Cd MNN induced) background spectrum (i.e., the spectrum of the 24 min – CdS/CIGSe^{NaF} sample and the 15 min – CdS/CIGSe^{NaF+KF} sample, respectively). For the CdS/CIGSe^{NaF} spectra one In MNN component (component In_a) and the background spectrum is sufficient to achieve a reasonable good fit, while for the CdS/CIGSe^{NaF+KF} data four different In MNN components (components In_a, In_b, In_c, and In_d – with at most two at the same time) are required. Vertical offsets are added for clarity.

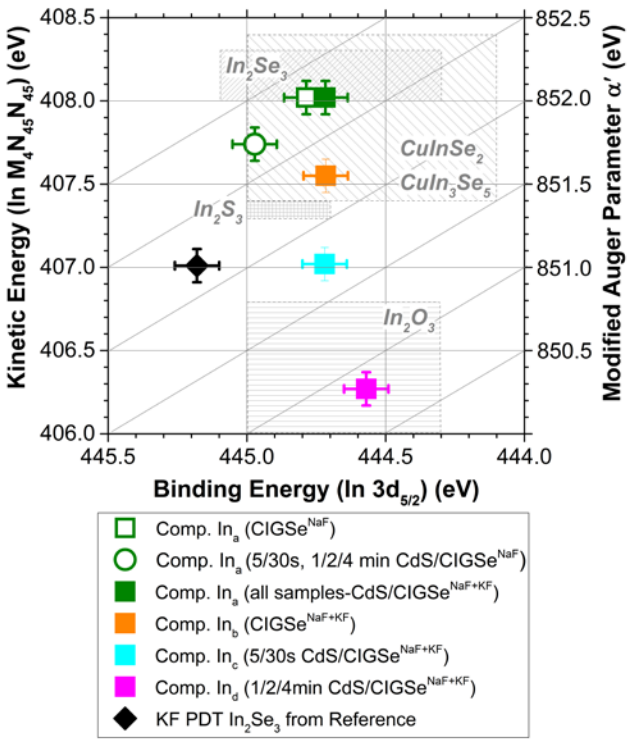

Figure 4. Evolution of the modified Auger parameter (α') of In [i.e., the sum of the binding energy (E_B) of the In $3d_{5/2}$ photoemission line and the kinetic energy (E_K) of the In $M_4N_{45}N_{45}$ Auger line] with increasing CdS CBD time. The KF-In_2Se_3 reference data point was adopted from Ref. [10]. For comparison, reference position area for In_2Se_3, $CuInSe_2$, $CuIn_3Se_5$, In_2S_3, and In_2O_3 compounds (as derived based on data in Ref. [36, 56-62] are indicated. The error bars are dominated by the uncertainty in the determination of the energy position of the individual components.

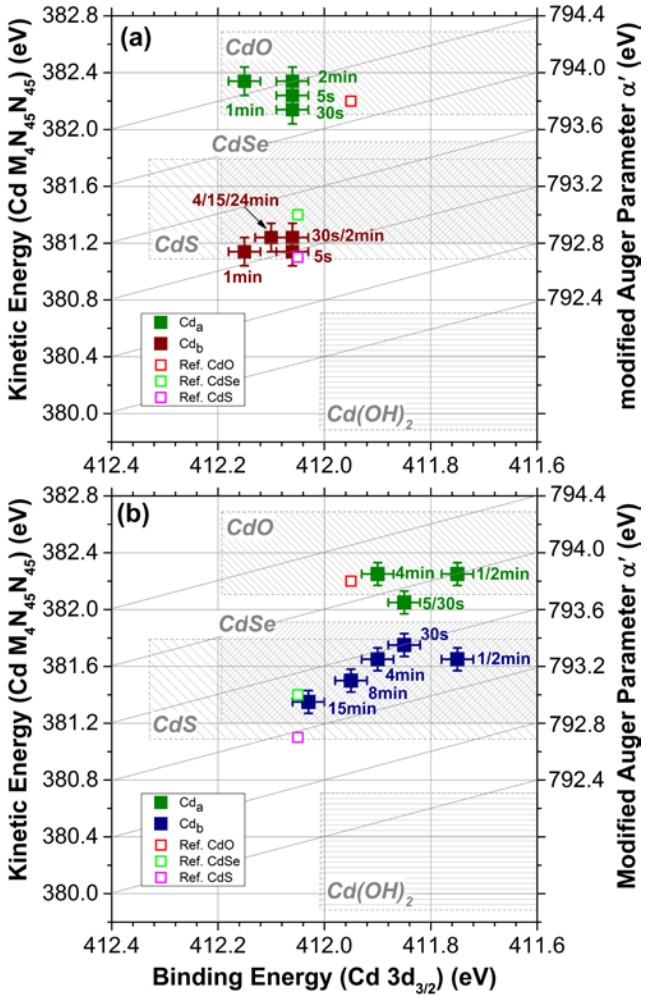

Figure 5. Evolution of the modified Auger parameter (α') of Cd [i.e., the sum of the binding energy (E_B) of the Cd $3d_{3/2}$ photoemission line and the kinetic energy (E_K) of the Cd $M_4N_{45}N_{45}$ Auger line] with increasing CBD time: (a) for the CdS/CIGSe^{NaF} and (b) for the CdS/CIGSe^{NaF+KF} sample set. Reference positions for CdO, CdS, CdSe, and $Cd(OH)_2$ compounds are indicated[34, 36-45]. The error bars are dominated by the uncertainty in the determination of the energy position of the individual components.

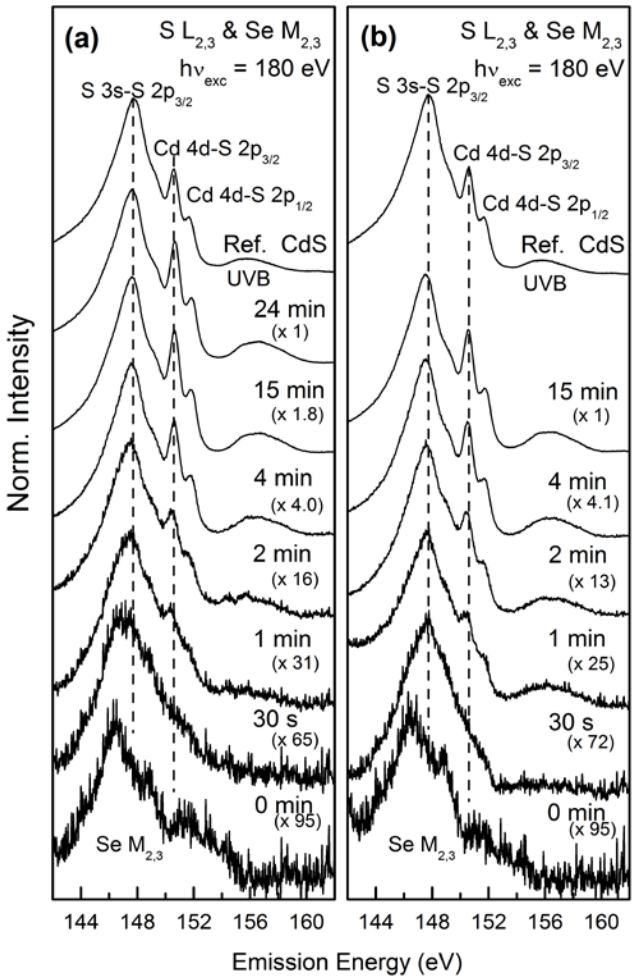

Figure 6. Background-normalized Se $M_{2,3}$/S $L_{2,3}$ XES spectra of the CdS/CIGSe^{NaF} (a) and CdS/CIGSe^{NaF+KF} (b) samples with increasing CdS-CBD time. CdS reference spectra[55] was added for comparison. The spectra are shown on different magnification scales (as indicated) and are vertically offset to allow for easy comparison.

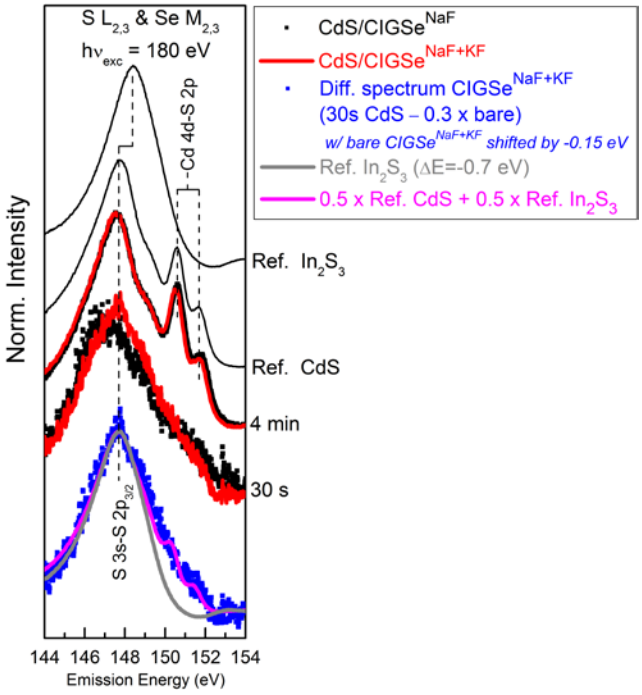

Figure 7. Direct comparison of four selected Se $M_{2,3}$/S $L_{2,3}$ XES spectra (30s and 4 min for both series) and the difference between bare and 30s CdS/CIGSe^{NaF+KF} are shown. A model "$CdIn_2S_4$" reference spectrum were produced by the S $L_{2,3}$ spectrum of 0.5 × CdS+0.5 × In_2S_3. All samples were excited at hν= 180 eV. Dashed lines are added as guides for spectral features and main features are labeled. CdS and In_2S_3 reference spectra[55] was added for comparison.

ASSOCIATED CONTENT

Supporting Information.

XPS survey spectra, photoemission data with respective Voigt fits for Mg K_α excitation, details for the In 4p and Cd 4p background subtraction procedure, effective buffer layer thickness calculation, area-normalized presentation & fit procedure of Se $M_{4,5}$ XES spectra, comparison of K 2p and O 1s-related contributions, background correction and fitting results of Cd MNN spectra, direct comparison of the S $L_{2,3}$/Se $M_{2,3}$ XES spectra to CdS/CIGSe samples.

AUTHOR INFORMATION

Corresponding Author

*E-mail: marcus.baer@helmholtz-berlin.de.

Author Contributions

The manuscript was written through contributions of all authors. All authors have given approval to the final version of the manuscript.

Notes

The authors declare no competing financial interest

ACKNOWLEDGMENT

The authors like to thank Dr. P. Reinhard, Dr. B. Bissig, Dr. E. Avancini, Dr. S. Buecheler, and Prof. A. N. Tiwari for making the samples available. The authors also acknowledge the support of Dr. D. Kreikemeyer-Lorenzo, Dr. L. Weinhardt, Dr. M. Blum, and Prof. C. Heske during the collection of the XES spectra. This work was supported in part by the Helmholtz-Association (VH-NG-423) and by the European Union's Horizon 2020 research and innovation program under grant agreement No 641004. P. Yang is also grateful to China Scholarship Council (CSC) for financial support.

REFERENCES

(1) Chirilă A.; Reinhard P.; Pianezzi F.; Bloesch P.; Uhl, A. R.; Fella C., Kranz L.; Keller D.; Gretener C.; Hagendorfer H.; Jaeger, D.; Erni, R.; Nishiwaki S.; Buecheler S.; Tiwari, A. N. Potassium-Induced Surface Modification of Cu(In,Ga)Se_2 Thin Films for High-Efficiency Solar Cells. *Nat. Mater*. **2013,** *12*, 1107-1111.
(2) Reinhard, P.; Bissig, B.; Pianezzi, F.; Avancini, E.; Hagendorfer, H.; Keller, D.; Fuchs, P.; Döbeli, M.; Vigo, C.; Crivelli, P.; Nishiwaki, S.; Buecheler, S.; Tiwari, A. N. Features of KF and NaF Postdeposition Treatments of Cu(In,Ga)Se_2 Absorbers for High Efficiency Thin Film Solar Cells. *Chem. Mater*. **2015,** *27*, 5755-5764.
(3) Jackson, P.; Wuerz, R.; Hariskos, D.; Lotter, E.; Witte, W.; Powalla, M. Effects of Heavy Alkali Elements in Cu(In,Ga)Se_2 Solar Cells with Efficiencies up to 22.6%. *Phys. Status Solidi RRL* **2016,** *10*, 583-586.
(4) Solar Frontier. http://www.solar-frontier.com/eng/news/2019/0117_press.html.
(5) Heske, C.; Fink, C.; Umbach, E.; Riedl, W.; Karg, F. Na Induced Effects on the Electronic Structure and Composition of Cu(In,Ga)Se_2 Thin Film Surfaces. *Appl. Phys. Lett.* **1996,** *68*, 3431-3433.

(6) Heske, C.; Eich, D.; Fink,R.; Umbach, E.; Kakar, S.; Van Buuren, T.; Bostedt, C.; Terminello, L. J.; Grush, M. M.; Callcott, T. A.; Himpsel, F. J.; Ederer, D. L.; Perera, R. C. C.; Riedl, W.; Karg, F. Localization of Na Impurities at the Buried CdS/Cu(In,Ga)Se_2 Heterojunction. *Appl. Phys. Lett.* **1999,** *75*, 2082-2084.
(7) Rudmann, D.; Brémaua, D.; Da Cunha, A. F.; Bilger, G.; Strohm, A.; Kaelin, M.; Zogg, H.; Tiwari, A. N. Sodium Incorporation Strategies for CIGS Growth at Different Temperatures. *Thin Solid Films* **2005,** *480–481*, 55-60.
(8) Hauschild, D.; Kreikemeyer-Lorenzo, D.; Jackson. P.; Magorian Friedlmeier, T.; Hariskos, D.; Reinert, F.; Powalla, M.; Heske, C.; Weinhardt L. Impact of a RbF Postdeposition Treatment on the Electronic Structure of the CdS/Cu(In,Ga)Se_2 Heterojunction in High-Efficiency Thin-Film Solar Cells. *ACS Energy Lett.* **2017,** *2*, 2383-2387.
(9) Contreras, M. A.; Romero, M. J.; to,B.; Hasoon, F.; Noufi, R.; Ward, S.; Ramanathan K. Optimization of CBD CdS Process in High-Efficiency Cu(In,Ga)Se_2-Based Solar Cells. *Thin Solid Films* **2002,** *403-404*, 204-211.
(10) Handick, E.; Reinhard, P.; Wilks, R. G.; Pianezzi, F.; Kunze, T.; Lorenzo, D. K.; Weinhardt, L.; Blum, M.; Yang, W.; Gorgoi, M.; Ikenaga, E.; Gerlach, D.; Ueda, S.; Yamashita, Y.;Chikyow, T.; Heske, C.; Buecheler, S.; Tiwari, A. N.; Bär, M. Formation of a K-In-Se Surface Species by NaF/KF PostdepositionTreatment of Cu(In,Ga)Se_2 Thin-Film Solar Cell Absorbers. *ACS Appl. Mater. Interfaces* **2017,** *9*, 3581-3589.
(11) Lundberg, O.; Wallin, E.; Gusak, V.; Södergren, S.; Chen, S.;Lotfi, S.; Chalvet, F.; Malm, U.; Kaihovirta, N.; Mende, P.;Jaschke, G.; Kratzert, P.; Joel, J.; Skupinski, M.; Lindberg, P.; Jarmar, T.; Lundberg, J.; Mathiasson, J.; Stolt, L., Improved CIGS Modules by KF Post Deposition Treatment and Reduced Cell-to-Module Losses. In *IEEE 43th Photovoltaic Specialists Conference (PVSC)*, IEEE: Portland, OR, USA, 2016 pp 1293-1296.
(12) Khatri, I.; Fukai, H.; Yamaguchi, H.; Sugiyama, M.; Nakada T. Effect of Potassium Fluoride Post-Deposition Treatment on Cu(In,Ga)Se_2 Thin Films and Solar Cells Fabricated onto Sodalime Glass Substrates. *Sol. Energy Mater. Sol. Cells* **2016,** *155*, 280-287.
(13) Lepetit, T. Influence of KF Post Deposition Treatment on the Polycrystalline Cu(In,Ga)Se_2/CdS Heterojunction Formation for Photovoltaic Application. Ph.D Thesis, Université de Nantes, 2015.
(14) Khatri, I.; Sugiyama, M.; Nakada, T. Effects of Combined Additional Indium Deposition and Potassium Fluoride Post-Deposition Treatments on Cu(In,Ga)Se_2 Thin Film Solar Cells. *Prog. Photovolt. Res. Appl.* **2017,** *25*, 871-877.
(15) Handick, E.; Reinhard, P.; Wilks, R. G.; Pianezzi, F.; Félix, R.; Gorgoi, M.; Kunze, T.; Buecheler, S.; Tiwari, A. N.; Bär M., NaF/KF Post-Deposition Treatments and Their Influence on the Structure of Cu(In,Ga)Se_2 Absorber Surfaces. In *IEEE 43th Photovoltaic Specialists Conference (PVSC)*, Portland, OR, USA, 2016; pp 0017-0021.
(16) Pistor, P.; Greiner, D.; Kaufmann, C. A.; Brunken, S.; Gorgoi, M.; Steigert, A.; Calvet, W.; Lauermann, I.; Klenk, R.; Unold, T.; Lux-Steiner, M.-C. Experimental Indication for Band Gap Widening of Chalcopyrite Solar Cell Absorbers after Potassium Fluoride Treatment. *Appl. Phys. Lett.* **2014,** *105*, 063901.
(17) Handick, E.; Reinhard, P.; Alsmeier, J.-H.; Köhler, L.; Pianezzi, F.; Krause, S.; Gorgoi, M.; Ikenaga, E.; Koch, N.; Wilks, R. G.; Buecheler, S.; Tiwari, A. N.; Bär, M. Potassium Postdeposition Treatment-Induced Band Gap Widening at Cu(In,Ga)Se_2 Surfaces-Reason for Performance Leap? *ACS Appl. Mater. Interfaces* **2015,** *7*, 27414-27420.

(18) Mezher, M.; Mansfield, L. M.; Horsley, K.; Blum, M.; Wieting, R.; Weinhardt, L.; Ramanathan, K.; Heske C. KF Post-Deposition Treatment of Industrial Cu(In, Ga)(S, Se)$_2$ Thin-Film Surfaces: Modifying the Chemical and Electronic Structure. *Appl. Phys. Lett.* **2017,** *111*, 071601.
(19) Nicoara, N.;Harel, S.; Lepetit, T.; Arzel, L.; Barreau, N.; Sadewasser, S. Impact of KF Post-Deposition Treatment on Aging of the Cu(In,Ga)Se$_2$ Surface and Its Interface with CdS. *ACS Appl. Energy Mater.* **2018,** *1*, 2681-2688.
(20) Avancini, E.; Carron, R.; Weiss, T. P.;Andres, C.; Burki, M.; Schreiner, C.; Figi, R.; Romanyuk, Y. E.; Buecheler, S.; Tiwari A. N. Effects of Rubidium Fluoride and Potassium Fluoride Postdeposition Treatments on Cu(In,Ga)Se$_2$ Thin Films and Solar Cell Performance. *Chem. Mater.* **2017,** *29*, 9695-9704.
(21) Briggs, D.; Seah, M. P. *Practical Surface Analysis: Auger and X-ray Photoelectron Spectroscopy*, Wiley: New York 1983.
(22) Wojdyra, M. Fityk: A General-Purpose Peak Fitting Program. *J. Appl. Crystallogr.* **2010,** *43*, 1126.
(23) Tanuma, S.; Powell, C. J.; Penn, D. R. Calculations of Electron Inelastic Mean Free Paths. *Surf. Interface Anal.* **1993,** *20*, 77-89.
(24) Weinhardt, L.; Fuchs, O.; Fleszar, A.; Bär, M.; Blum, M.; Weigand, M.; Denlinger, J. D.; Yang, W.; Hanke, W.; Umbach, E.; Heske, C. Resonant Inelastic Soft X-ray Scattering of CdS: A Two-Dimensional Electronic Structure Map Approach. *Phys. Rev. B* **2009,** *79*, 165305.
(25) Henke, B. L.; Gullikson, E. M.; Davis, J. C. CXRO Database for the X-ray Attenuation Length of a Solid. http://henke.lbl.gov/optical_constants/atten2.html.
(26) Reinhard, P.; Pianezzi, F.; Bissig, B.; Chiril, A.; Buecheler, S.; Tiwari, A. N. . Cu(In,Ga)Se$_2$ Thin-Film Solar Cells and Modules—A Boost in Efficiency Due to Potassium. *IEEE J. Photovoltaics* **2014,** *5*, 656-663.
(27) Pianezzi, F.; Reinhard, P.; Chirilă, A.; Bissig, B.; Nishiwaki, S.; Buecheler, S.; Tiwari, A. N. Unveiling the Effects of Post-Deposition Treatment with Different Alkaline Elements on the Electronic Properties of CIGS Thin Film Solar Cells. *Phys. Chem. Chem. Phys.* **2014,** *16*, 8843-8851.
(28) Trzhaskovskaya, M. B. Photoelectron Angular Distribution Parameters for Elements Z= 1 to Z=54 in the Photoelectron Energy Range 100-5000eV. *At. Data Nucl. Data Tables* **2001,** *77*, 97-159.
(29) Malitckaya, M.; Kunze, T.; Komsa, H.-P.; Havu, V.; Handick, E.; Wilks, R. G.; Bär, M.; Puska, M. J. Alkali Postdeposition Treatment-Induced Changes of the Chemical and Electronic Structure of Cu(In,Ga)Se$_2$ Thin-Film Solar Cell Absorbers: A First-Principle Perspective. *ACS Appl. Mater. Interfaces* **2019,** *11*, 3024-3033.
(30) Weinhardt, L.; Bär, M.; Pookpanratana, S.; Morkel, M.; Niesen, T. P.; Karg, F.; Ramanathan, K.; Contreras, M. A.; Noufi, R.; Umbach, E.; Heske C. Sulfur Gradient-Driven Se Diffusion at the CdS/CuIn(S,Se)$_2$ Solar Cell Interface. *Appl. Phys. Lett.* **2010,** *96*, 182102.
(31) Bär, M.; Weinhardt, L.; Heske, C.; Muffler, H.-J.; Lux-Steiner, M. Ch.; Umbach, E.; Fischer Ch.-H. Cd^{2+}/NH_3 Treatment of Cu(In,Ga)(S,Se)$_2$ Thin-film Solar Cell Absorbers: A Model for the Performance-enhancing Processes in the Partial Electrolyte. *Prog. Photovolt. Res. Appl.* **2005,** *13*, 571-577.
(32) Bär, M.; Repins, I.; Weinhardt, L.; Alsmeier, J.-H.; Pookpanratana, S.; Blum, M.; Yang, W.; Heske, C.; Wilks, R. G.; Nouf, R. Zn−Se−Cd−S Interlayer Formation at the CdS/$Cu_2ZnSnSe_4$ Thin-Film Solar Cell Interface. *ACS Energy Lett.* **2017,** *2*, 1632-1640.

(33) Wagner, C. D. Chemical Shifts of Auger Lines, and the Auger Parameter. *Faraday Discuss. Chem. Soc.* **1975,** *60*, 291-300.
(34) Gaarenstroom, S. W.; Winograd, N. Initial and Final State Effects in the ESCA Spectra of Cadmium and Silver Oxides. *J. Chem. Phys.* **1977,** *67*, 3500-3506.
(35) Wagner, C. D.; Gale, L. H.; Raymond, R. H. Two-Dimensional Chemical State Plots: A Standardized Data Set for Use in Identifying Chemical States by X-Ray Photoelectron Spectroscopy. *Ana. Chem.* **1979,** *51*, 466-482.
(36) Moulder, J. F.; Stickle, W. F.; Sobol, P. E.; Bomben, K. D. *Handbook of X-Ray Photoelectron Spectroscopy*, Minnesota, USA, 1995.
(37) Niles, D. W.; Herdt, G.; Al-Jassim, M. An X-ray Photoelectron Spectroscopy Investigation of O Impurity Chemistry in CdS Thin Films Grown by Chemical Bath Deposition. *J. Appl. Phys.* **1997,** *81*, 1978-1984.
(38) Bhide, V. G.; Salkalachen, S.; Rastog, A. C.; Rao, C. N. R.; Hegde, M. S. Depth Profile Composition Studies of Thin Film CdS:Cu_2S Solar Cells Using XPS and AES. *J. Phys. D: Appl. Phys.* **1981,** *14*, 1647-1656.
(39) Riga, J.; Verbist, J. J.; Josseaux, P.; Mesmaeker, A. K. Correlation between CdS Photoanodic Behaviour and Electrode Chemical Modifications: An X-ray Photoelectron Spectroscopic Study. *Surf. Interface Anal.* **1985,** *7*, 163-168.
(40) Wagner C.D.; Gale L. H.; Raymond, R. H. Two-Dimensional Chemical State Plots: A Standardized Data Set for Use in Identifying Chemical States by X-ray Photoelectron Spectroscopy. *Ana. Chem.* **1979,** *51*, 466-482.
(41) Tkachenko, O. P.; Shpiro, E. S.; Wark, M.; Ekloff, G. S.; Jaeger, N. X-Ray Photoelectron/X-Ray Excited Auger Electron Spectroscopic Study of Highly Dispersed Semiconductor CdS and CdO Species in Zeolites. *J. Chem. Soc. Faraday Trans.* **1993,** *89*, 3987-3994.
(42) Polak, M. X-Ray Photoelectron Spectroscopic Studies of $CdSe_{0.65}Te_{0.35}$. *J. Electron. Spectrosc. Relat. Phenom.* **1982,** *28*, 171-176.
(43) Banerjeea, S.; Wong, S. S. Formation of CdSe Nanocrystals onto Oxidized, Ozonized Single-Walled Carbon Nanotube Surfaces. *ChemComm* **2004**, 1866-1867.
(44) Zhang, D. E.; Pan, X. D.; Zhu, H.; Li, S. Z.; Xu, G. Y.; Zhang, X. B.; Ying, A. L.; Tong, Z. W. A Simple Method to Synthesize Cadmium Hydroxide Nanobelts. *Nanoscale Res. Lett.* **2008,** *3* (8), 284-288.
(45) Islam, R.; Rao, D. R. X-ray Photoelectron Spectroscopy of $Zn_{1-x}Cd_xSe$ Thin Films. *J. Electron. Spectrosc. Relat. Phenom.* **1996,** *81*, 69-77.
(46) Fantauzzi, M.; Elsener, B.; Atzei, D.; Rigoldiab, A.; Rossi A. Exploiting XPS for the Identification of Sulfides and Polysulfides. *RSC Adv.* **2015,** *5*, 75953-75963.
(47) Weinhardt, L.; Fuchs, O.; Umbach, E.; Heske, C.; Fleszar, A.; Hanke, W.;Denlinger, J. D. Resonant Inelastic Soft X-ray Scattering, X-ray Absorption Spectroscopy, and Density Functional Theory Calculations of the Electronic Bulk Band Structure of CdS. *Phys. Rev. B* **2007,** *75*, 165207.
(48) Zhou, L.; Callcott, T. A.; Jia, J. J.; Ederer, D. L.; Perera, R. Sulfur $L_{2,3}$ and Zinc $M_{2,3}$ Soft-X-ray Fluorescence Spectra in CdS and ZnS. *Phys. Rev. B* **1997,** *55*, 5051-5061.
(49) Hubbell, J. H.; Trehan, P. N.; Singh, Nirmal; Chand, B.; Mehta, D.; Garg, M. L.; Garg, R. R.; Singh, Surinder; Puri, S. A Review, Bibliography, and Tabulation of K, L, and Higher Atomic Shell X-Ray Fluorescence Yields. *J. Phys. Chem. Ref. Data* **1994,** *23*, 339-364.
(50) National Institute of Standards and Technology. https://srdata.nist.gov/xps/.

(51) Pookpanratana, S.; Repins, I.; Bär, M.; Weinhardt, L.; Zhang, Y.; Félix, R.; Blum, M.; Yang, W.; Heske C. CdS/Cu(In,Ga)Se_2 Interface Formation in High-Efficiency Thin Film Solar Cells. *Appl. Phys. Lett.* **2010,** *97*, 074101.
(52) Meisel, A.; Leonhardt, G.; Szargan, R. *X-Ray Spectra and Chemical Binding; Springer Series in Chemical Physic*, Springer-Verlag: Berlin, 1989; Vol. 37, p 458.
(53) Heske, C.; Eich, D.; Fink, R.; Umbach, E.; Van Buuren,T.; Bostedt, C.; Terminello, L. J.; Kakar, S.; Grush, M. M.; Callcott, T. A.; Himpsel, F. J.; Ederer, D. L.; Perera, R. C. C.; Riedl, W.; Karg F. Observation of Intermixing at the Buried CdS/Cu(In,Ga)Se_2 Thin Film Solar Cell Heterojunction. *Appl. Phys. Lett.* **1999,** *74*, 1451-1453.
(54) Reichardt, J.; Bär, M.; Grimm, A.; Kötschau, I.; Lauermann, I.; Sokoll, S.; Lux-Steiner, M. C.; Fischer, Ch. H.; Heske, C.; Weinhardt, L.; Fuchs, O.; Jung, Ch.; Gudat, W.; Niesen, T. P.; Karg F. Inducing and Monitoring Photoelectrochemical Reactions at Surfaces and Buried Interfaces in Cu(In,Ga)$(S,Se)_2$ Thin-Film Solar Cells. *Appl. Phys. Lett.* **2005,** *86*, 172102.
(55) Duarte, R. F. Analysis and Optimization of Interfaces in "Wide-Gap" Chalcopyrite-based Thin Film Solar Cell Devices. Ph.D Thesis, BTU Cottbus-Senftenberg, 2015.
(56) Kazmerski L. L.; Jamjoum O.; Ireland P. J.; Deb, S. K. R.; Mickelsen A.; Chen W. Initial Oxidation of $CuInSe_2$. *J. Vacuum Sci. & Technol.* **1981,** *19*, 467-471.
(57) Cahen, D.; Ireland, P. J.; Kazmerski, L. L.; Thiele, F. A. X-ray Photoelectron and Auger Electron Spectroscopic Analysis of Surface Treatments and Electrochemical Decomposition of $CuInSe_2$ Photoelectrodes. *J. Appl. Phys.* **1985,** *57* (10), 4761-4771.
(58) Von Morzé, N.; Dittrich, T.; Calvet, W.; Lauermann, I.; Rusu M. Transient and Modulated Charge Separation at $CuInSe_2$/C60 and $CuInSe_2$/ZnPc Hybrid Interfaces. *Appl. Surf. Sci.* **2017,** *396*, 366-374.
(59) Faur, M.; Jayne, D. T.; Goradia, M.; Goradia, C. XPS Investigation of Anodic Oxides Grown on P-type InP. *Surf. Interface Anal.* **1990,** *15*, 641-650.
(60) Lin, A. W. C.; Armstrong N. R.; Kuwana, T. X-ray Photoelectron/Auger Electron Spectroscopic Studies of Tin and Indium Metal Foils and Oxides. *Ana. Chem.* **1977,** *49*, 1228-1235.
(61) Bertrand, P. A. XPS Study of Chemically Etched GaAs and InP. *J. Vacuum Sci. & Technol.* **1981,** *18*, 28-33.
(62) Sterner, J.; Malmström, J.; Stolt, L. Study on ALD In_2S_3/Cu(In,Ga)Se_2 Interface Formation. *Prog. Photovolt. Res. Appl.* **2005,** *13*, 179-193.

TOC figure

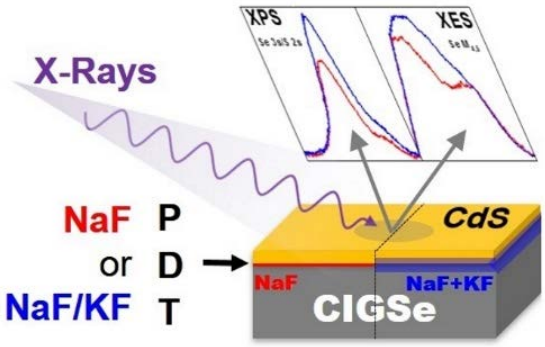

Supplementary Information

Interface Formation between CdS and Alkali Post-Deposition Treated $Cu(In,Ga)Se_2$ Thin Film Solar Cell Absorbers – Key to Understanding the Efficiency Gain?

Penghui Yang,[†] *Regan G. Wilks,*[†,‡] *Wanli Yang,*[§] *and Marcus Bär*[*,†,‡,∥,#]

[†]Dept. Interface Design, Helmholtz-Zentrum Berlin für Materialien und Energie GmbH, 12489 Berlin, Germany.

[‡]Energy Materials In-Situ Laboratory Berlin (EMIL), Helmholtz-Zentrum Berlin für Materialien und Energie GmbH, Berlin, 12489 Berlin, Germany.

[§]Advanced Light Source Lawrence Berkeley National Laboratory, Berkeley, CA 94720, USA

[∥]Department of Chemistry and Pharmacy, Friedrich-Alexander-Universität Erlangen-Nürnberg, Egerlandstr. 3, 91058 Erlangen, Germany

[#]Helmholtz Institute Erlangen-Nürnberg für Renewable Energy (HI-ERN), Albert-Einstein-Str. 15, 12489 Berlin, Germany

Corresponding Author

*E-mail: marcus.baer@helmholtz-berlin.de.

1. Basic principles of the used characterization techniques

When an x-ray photon impinges on a material surface, it interacts with the sample. In general, this causes electrons to be excited from an occupied to an unoccupied electronic state or (if the excitation energy is sufficient, i.e. > than the electron binding energy + the work function of the sample) to leave the sample. The remaining kinetic energy of these photoelectrons is then measured by, e.g. an electron analyzer. Since the electron's binding energy (and thus the measured kinetic energy) is element specific, the chemical composition of the sample can be probed that way. Due to the short inelastic mean free path (IMFP) of electrons at kinetic energies attainable with soft x-ray excitation, laboratory-based x-ray photoelectron spectroscopy measurements (XPS, generally using Mg K_α or Al K_α excitation) give a surface-sensitive view of the elements present in the sample. Since the intensity of the XPS line is directly related to the amount of the element present in the sample, the (surface) composition of the studied sample can (under certain assumptions, see e.g. Ref.[1] for more details) be derived. Furthermore, since the binding energy of a core electron of an element is influenced by the chemical bonding of that element (due to e.g. changes in electrostatic shielding upon bond formation – induced changes in the valence electron density of states), careful analysis of energy position and spectral shape of the measured XPS lines will also give insights into the chemical environment of the probed element.

In the x-ray emission process, the core hole created upon x-ray irradiation induced electron excitation (see above) is filled by a lower binding-energy electron, causing the emission of a photon. In x-ray emission spectroscopy (XES), the thus emitted photons are probed by a wavelength-dispersive x-ray spectrometer. Since XES is element-specific, it is an excellent tool to probe the local chemical structure. The probability for this process is very small; therefore, the experiment has to be performed at high-brightness synchrotron radiation sources. Since XES is a photon-in – photon-out process, its information depth is governed by the x-ray

attenuation length in the probed material and thus approximately 1 – 2 orders of magnitude larger than that of XPS (for more details see Ref.[2]).

2. Survey and detail spectra: Quantification

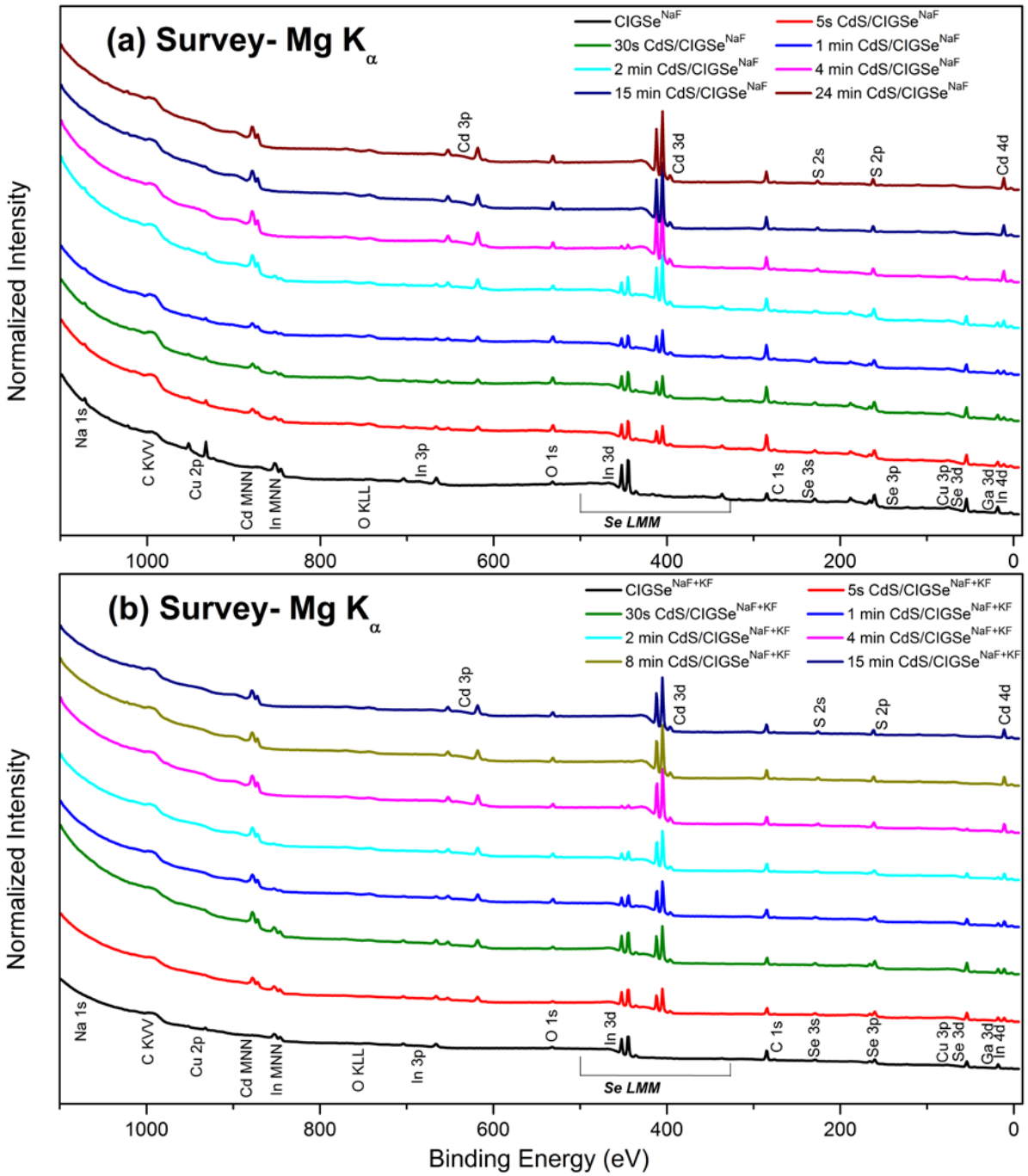

Figure S1. XPS survey spectra (normalized to background at a binding energy of 0 eV) of CdS/CIGSe^{NaF} (a) and CdS/CIGSe^{NaF+KF} (b) with increasing CBD time (varied between 0 and 24 [15] min). All the spectra were measured with excitation energies of hν=1253.56 eV (Mg K_α). All prominent photoemission and Auger lines are labeled. Spectra are vertically offset for clarity.

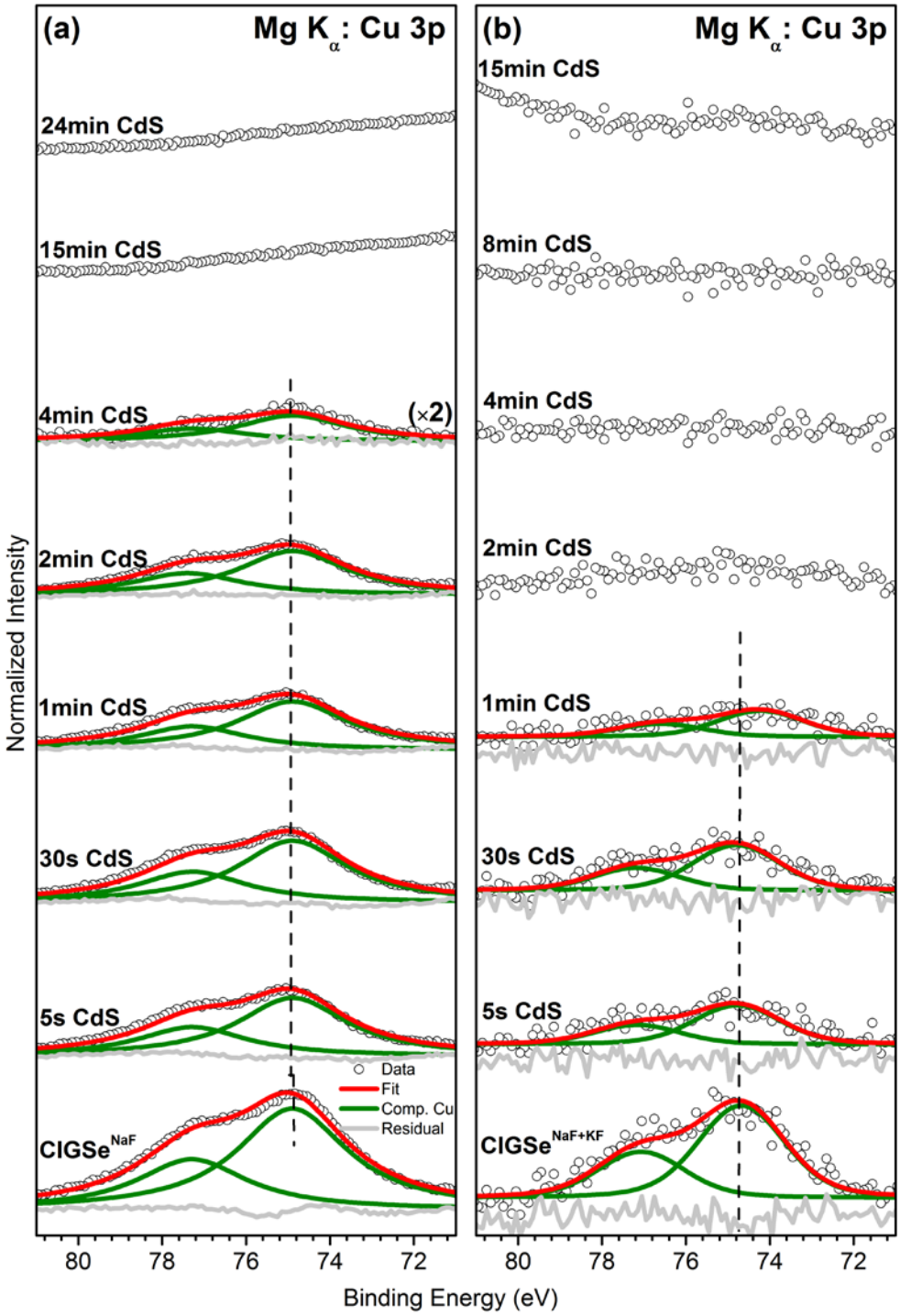

Figure S2. Cu 3p XPS data with respective Voigt fits of the CdS/CIGSe^{NaF} (a) and CdS/CIGSe^{NaF+KF} (b) sample series, measured with excitation energies of 1253.56 eV (Mg K_α). All spectra are displayed after subtraction of a linear background. For each fit, the residual is shown as well. Note the different magnification factors. Spectra are vertically offset for clarity.

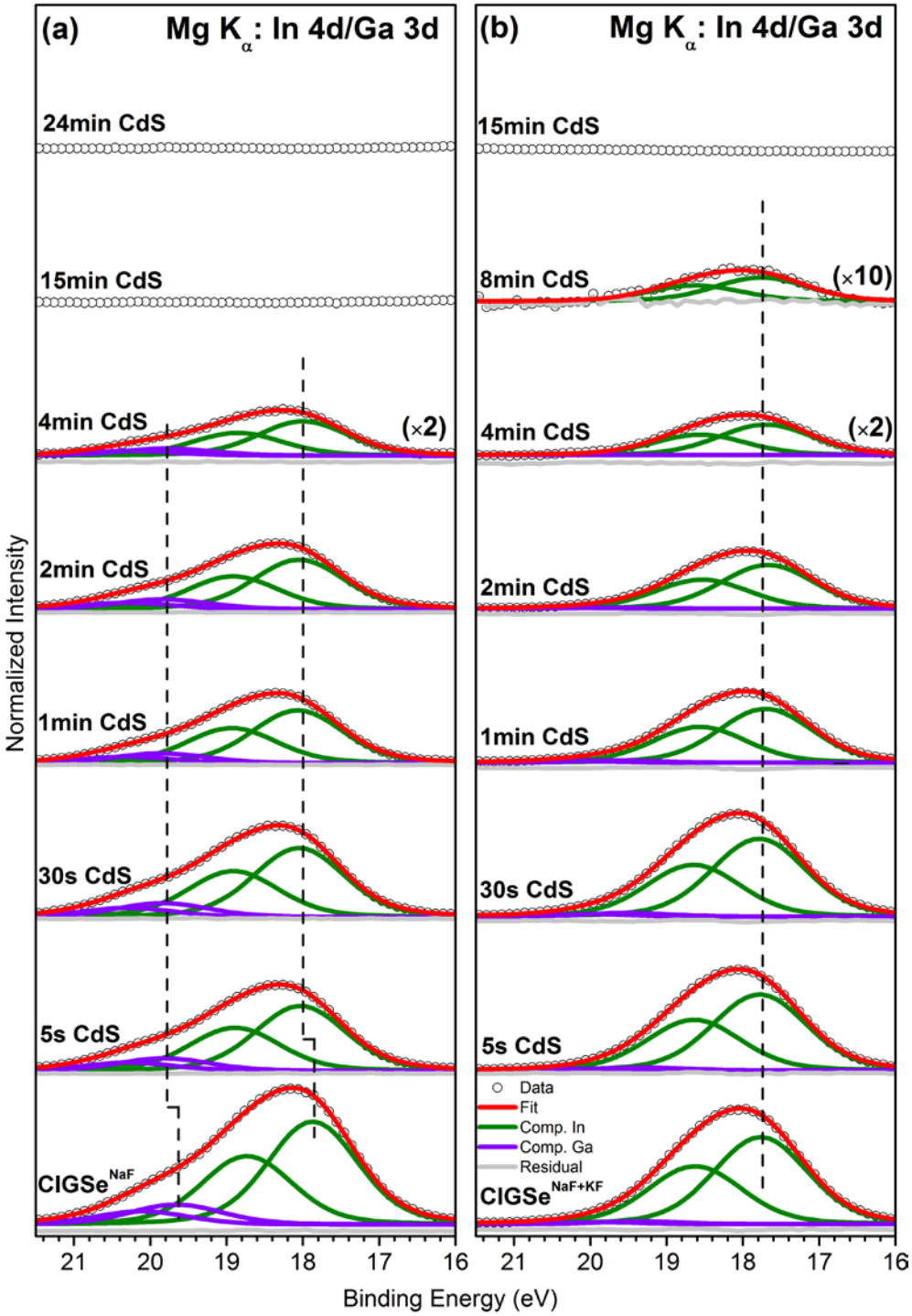

Figure S3. In 4d/Ga 3d XPS data with respective Voigt fits of the CdS/CIGSe^{NaF} (a) and CdS/CIGSe^{NaF+KF} (b) sample series, measured with excitation energies of 1253.56 eV (Mg K_α). All spectra are displayed after subtraction of a linear background. For each fit, the residual is shown as well. Note the different magnification factors. Spectra are vertically offset for clarity.

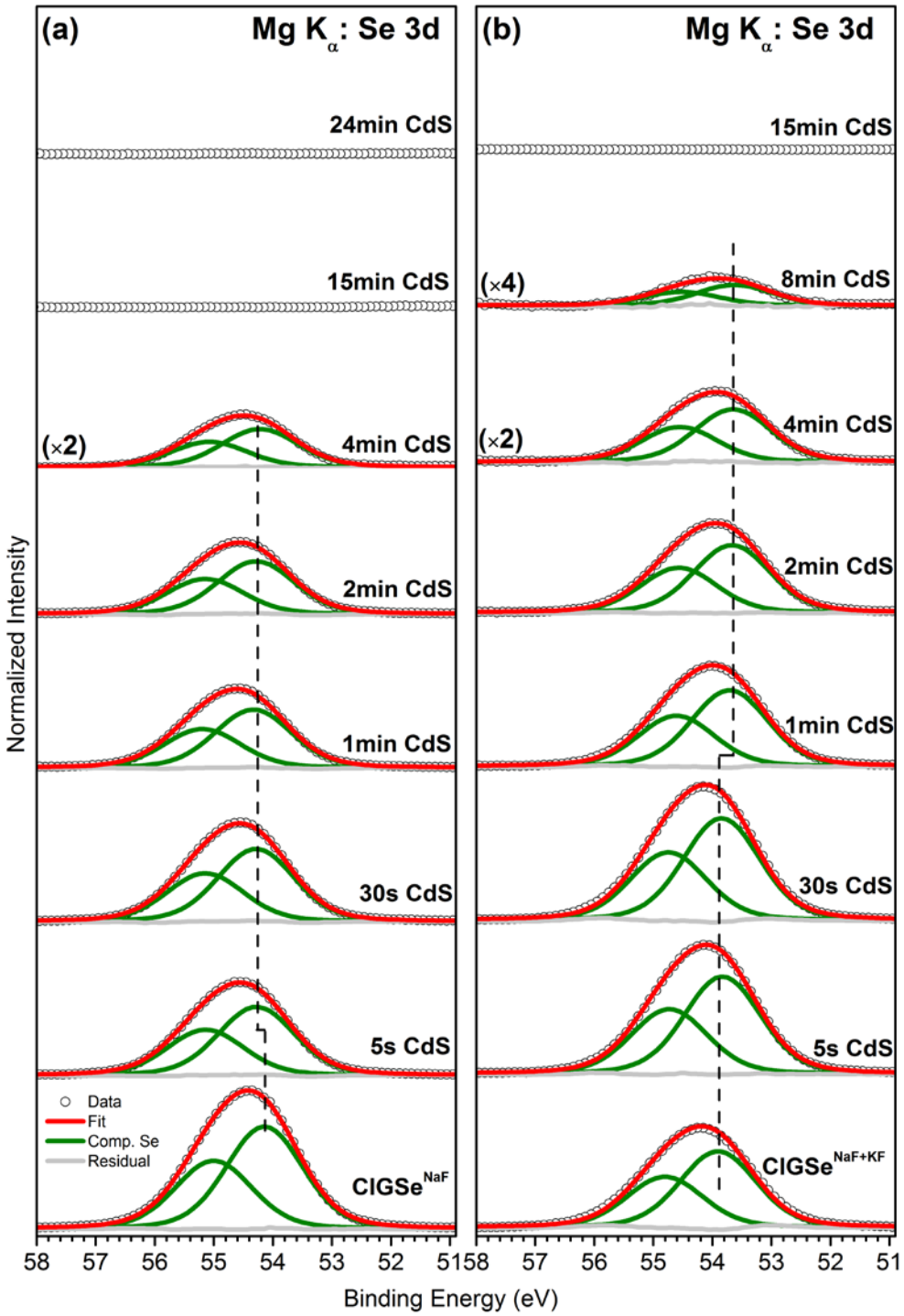

Figure S4. Se 3d XPS data with respective Voigt fits of the CdS/CIGSe^{NaF} (a) and CdS/CIGSe^{NaF+KF} (b) sample series, measured with excitation energies of 1253.56 eV (Mg K_α). All spectra are displayed after subtraction of a linear background. For each fit, the residual is shown as well. Note the different magnification factors. Spectra are vertically offset for clarity.

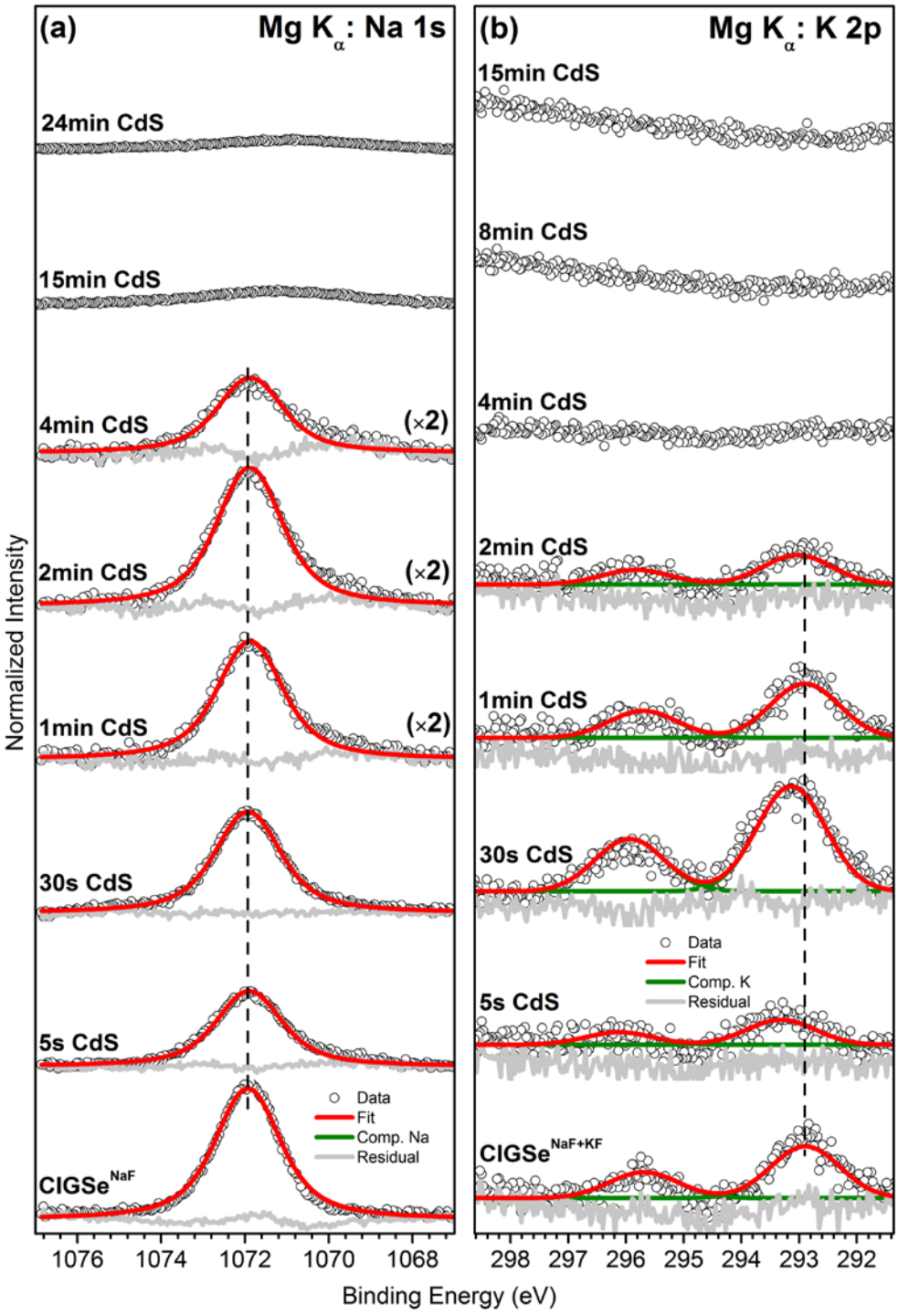

Figure S5. Na 1s (a) and K 2p (b) XPS data with respective Voigt fits of the CdS/CIGSe^{NaF} (a) and CdS/CIGSe^{NaF+KF} (b) sample series, measured with excitation energies of 1253.56 eV (Mg K_α). All spectra are displayed after subtraction of a linear background. For each fit, the residual is shown as well. Note the different magnification factors. Spectra are vertically offset for clarity.

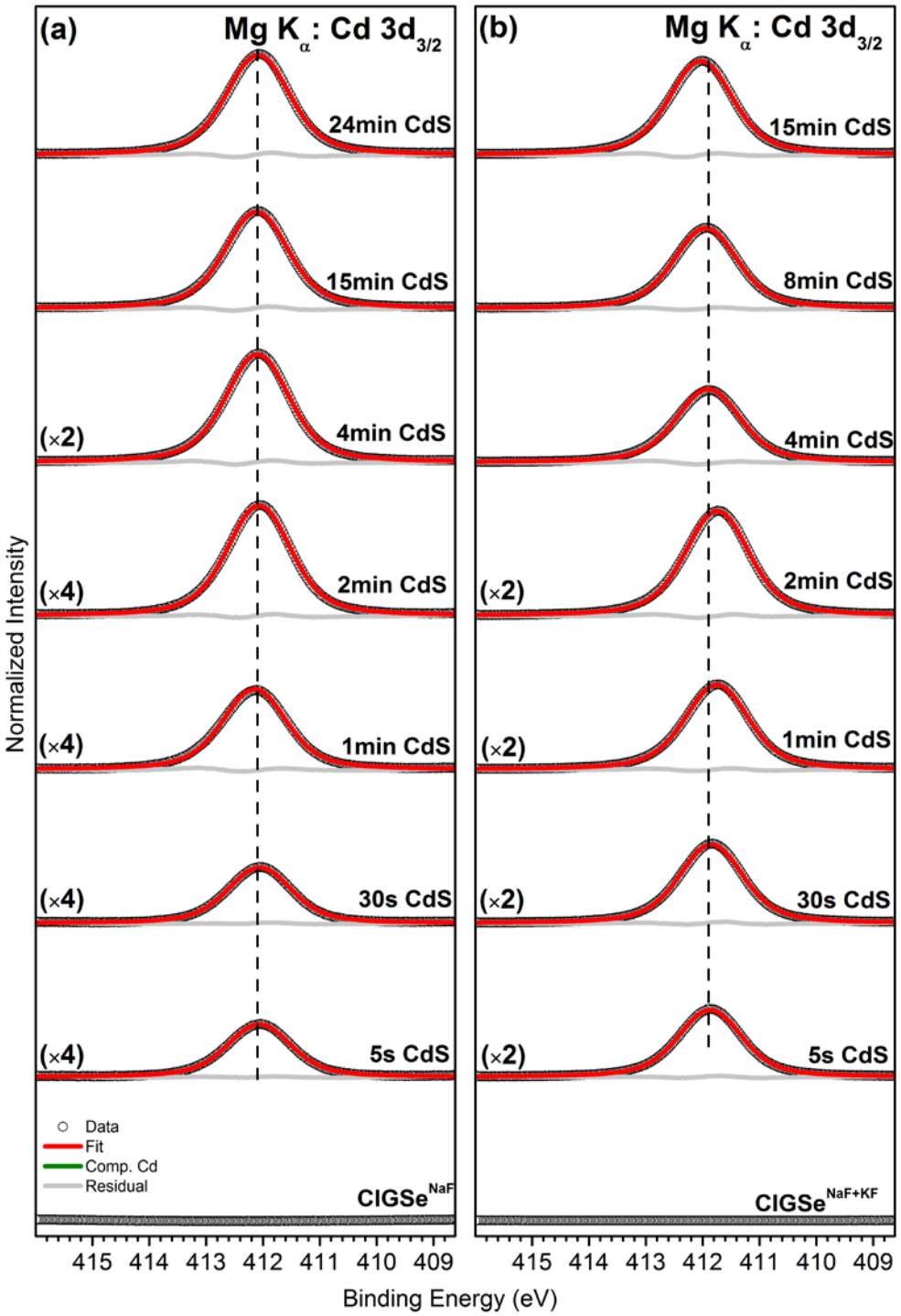

Figure S6. Cd 3d XPS data with respective Voigt fits of the CdS/CIGSe^{NaF} (a) and CdS/CIGSe^{NaF+KF} (b) sample series, measured with excitation energies of 1253.56 eV (Mg K_α). All spectra are displayed after subtraction of a linear background. For each fit, the residual is shown as well. Note the different magnification factors. Spectra are vertically offset for clarity.

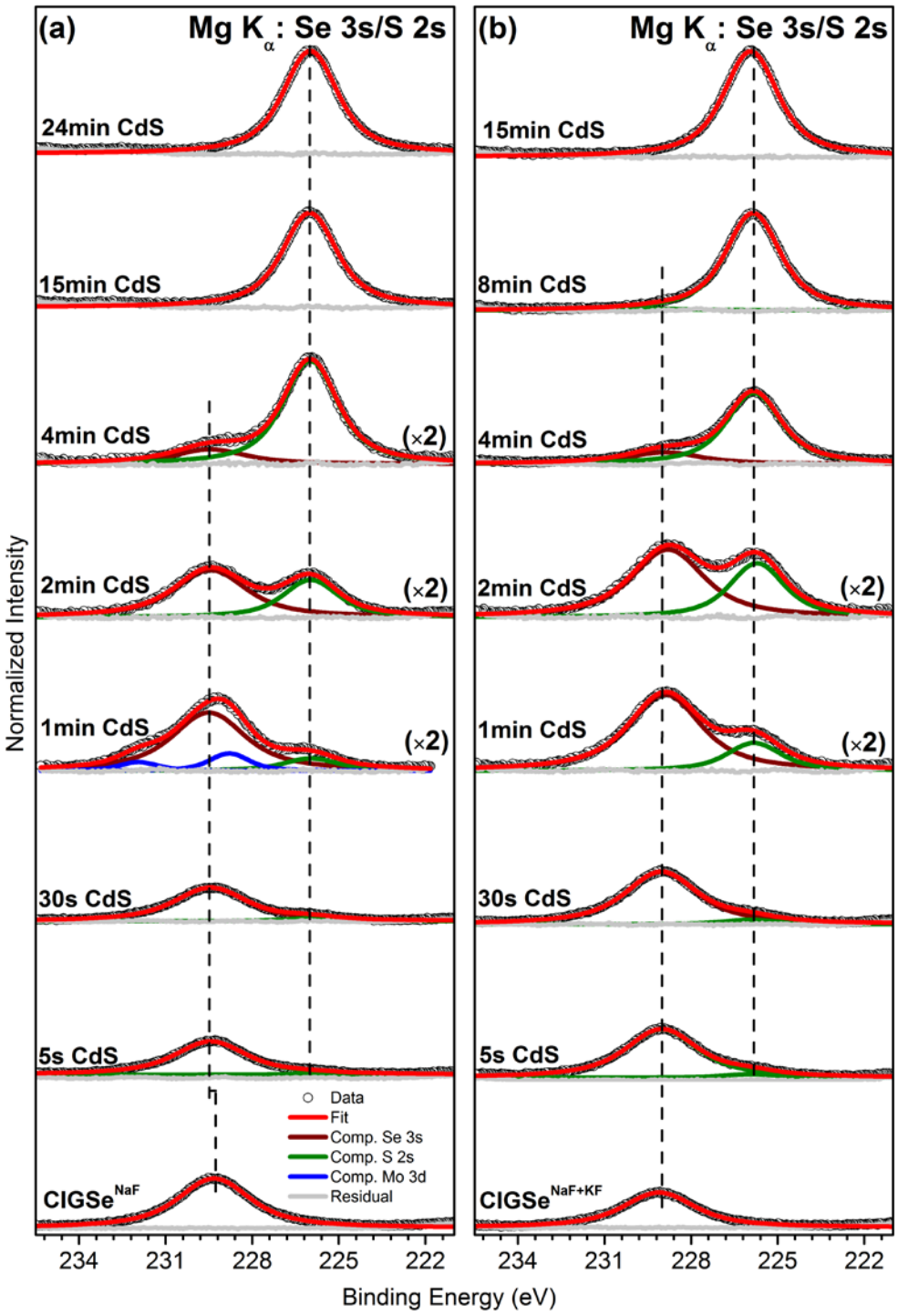

Figure S7. Se 3s/S 2s XPS data with respective Voigt fits of the CdS/CIGSe^{NaF} (a) and CdS/CIGSe^{NaF+KF} (b) sample series, measured with excitation energies of 1253.56 eV (Mg K_α). All spectra are displayed after subtraction of a linear background. For each fit, the residual is shown as well. Note the different magnification factors. Spectra are vertically offset for clarity.

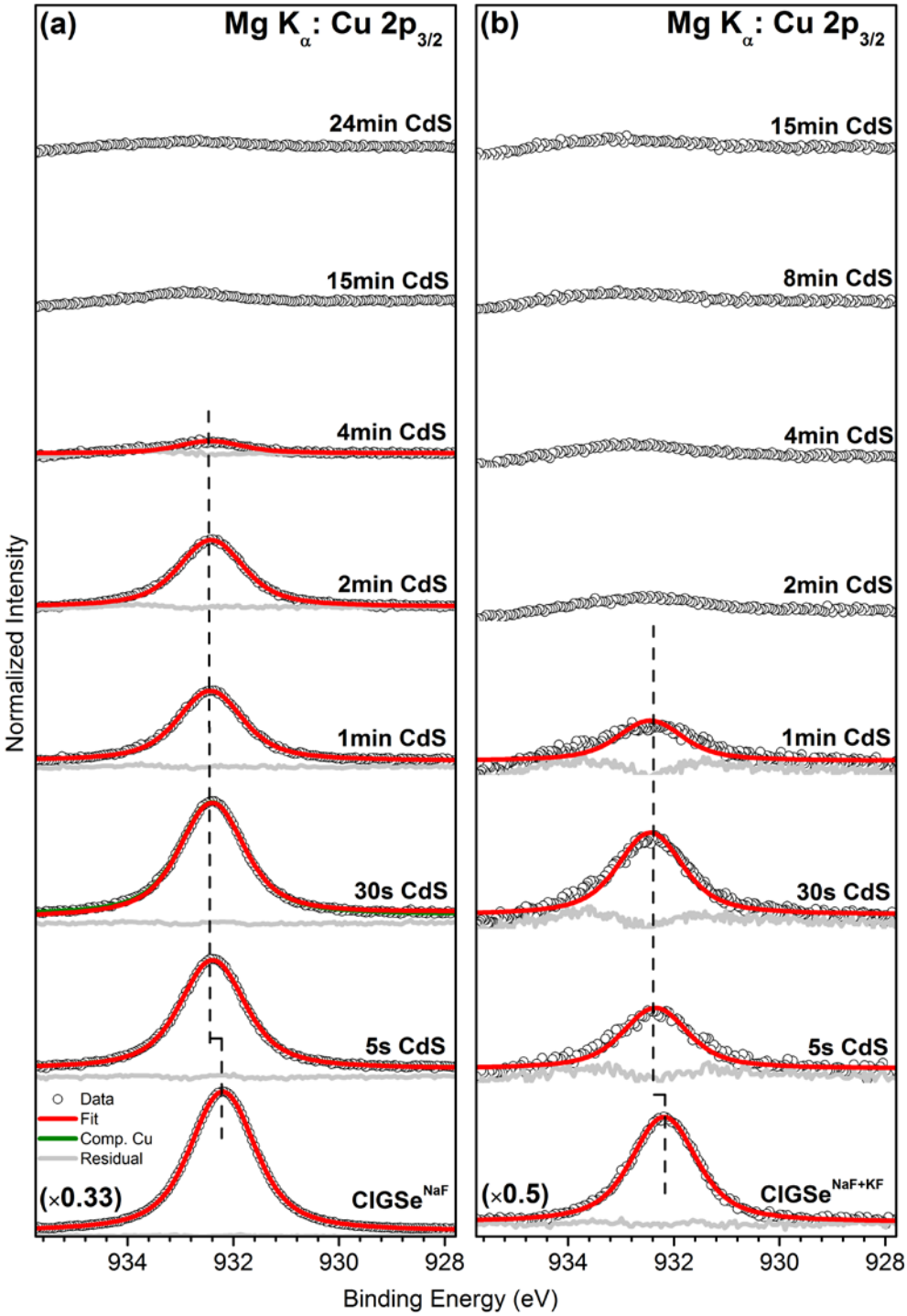

Figure S8. Cu $2p_{3/2}$ XPS data with respective Voigt fits of the CdS/CIGSe^{NaF} (a) and CdS/CIGSe^{NaF+KF} (b) sample series, measured with excitation energies of 1253.56 eV (Mg K_α). All spectra are displayed after subtraction of a linear background. For each fit, the residual is shown as well. Note the different magnification factors. Spectra are vertically offset for clarity.

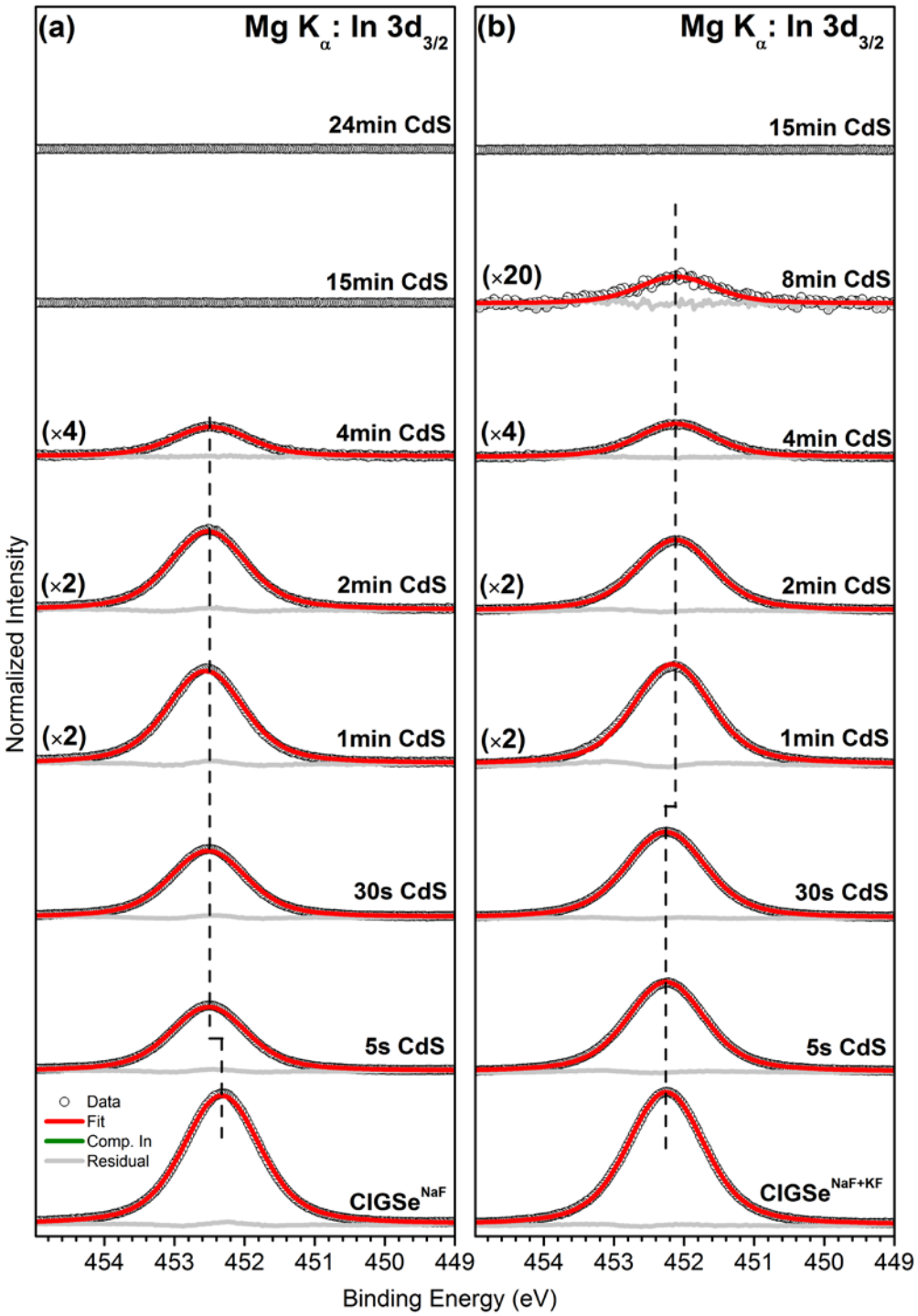

Figure S9. In $3d_{3/2}$ XPS data with respective Voigt fits of the CdS/CIGSe^{NaF} (a) and CdS/CIGSe^{NaF+KF} (b) sample series, measured with excitation energies of 1253.56 eV (Mg K_α). All spectra are displayed after subtraction of a linear background. For each fit, the residual is shown as well. Note the different magnification factors. Spectra are vertically offset for clarity.

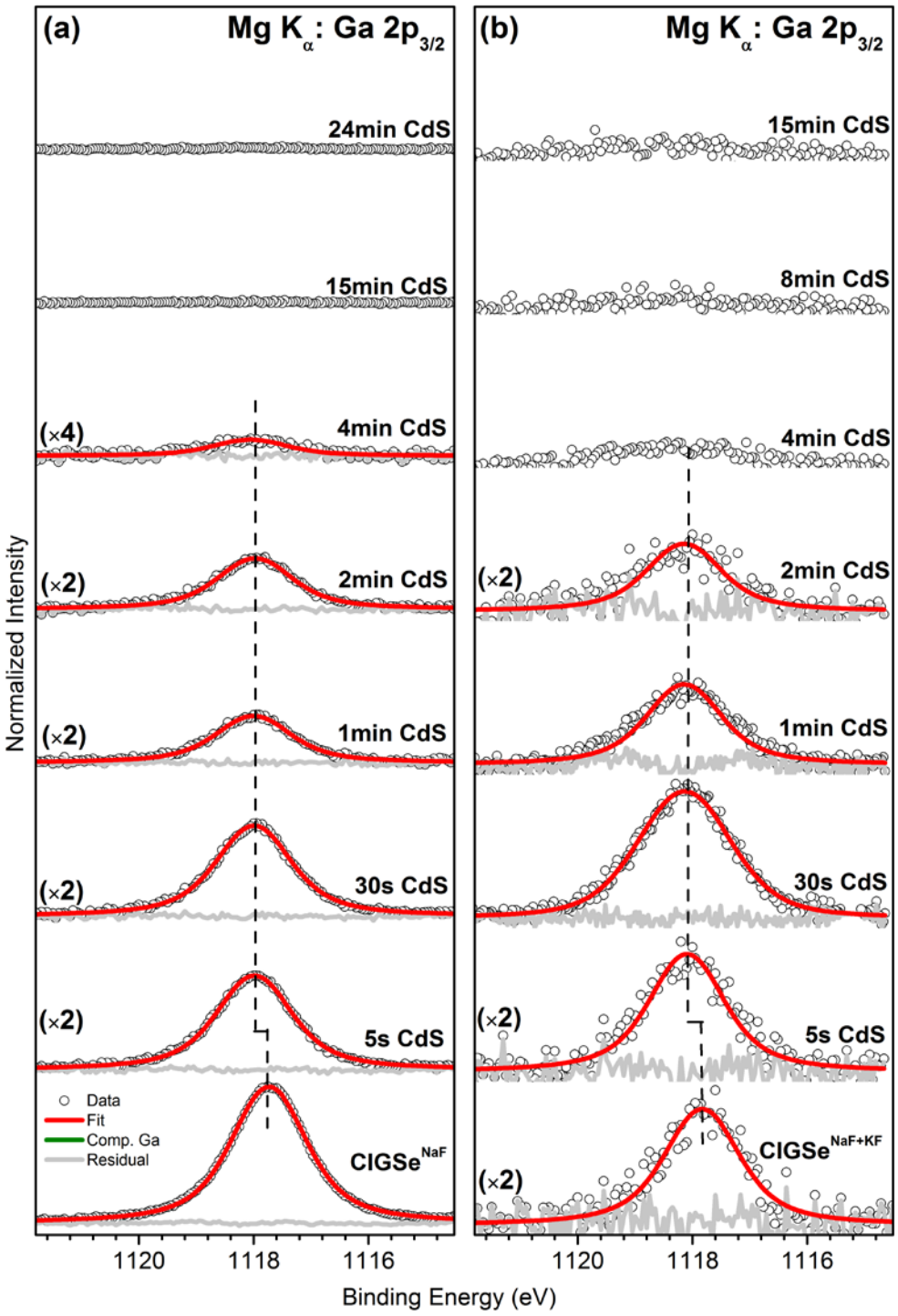

Figure S10. Ga 2p$_{3/2}$ XPS data with respective Voigt fits of the CdS/CIGSe^{NaF} (a) and CdS/CIGSe^{NaF+KF} (b) sample series, measured with excitation energies of 1253.56 eV (Mg K$_\alpha$). All spectra are displayed after subtraction of a linear background. For each fit, the residual is shown as well. Note the different magnification factors. Spectra are vertically offset for clarity.

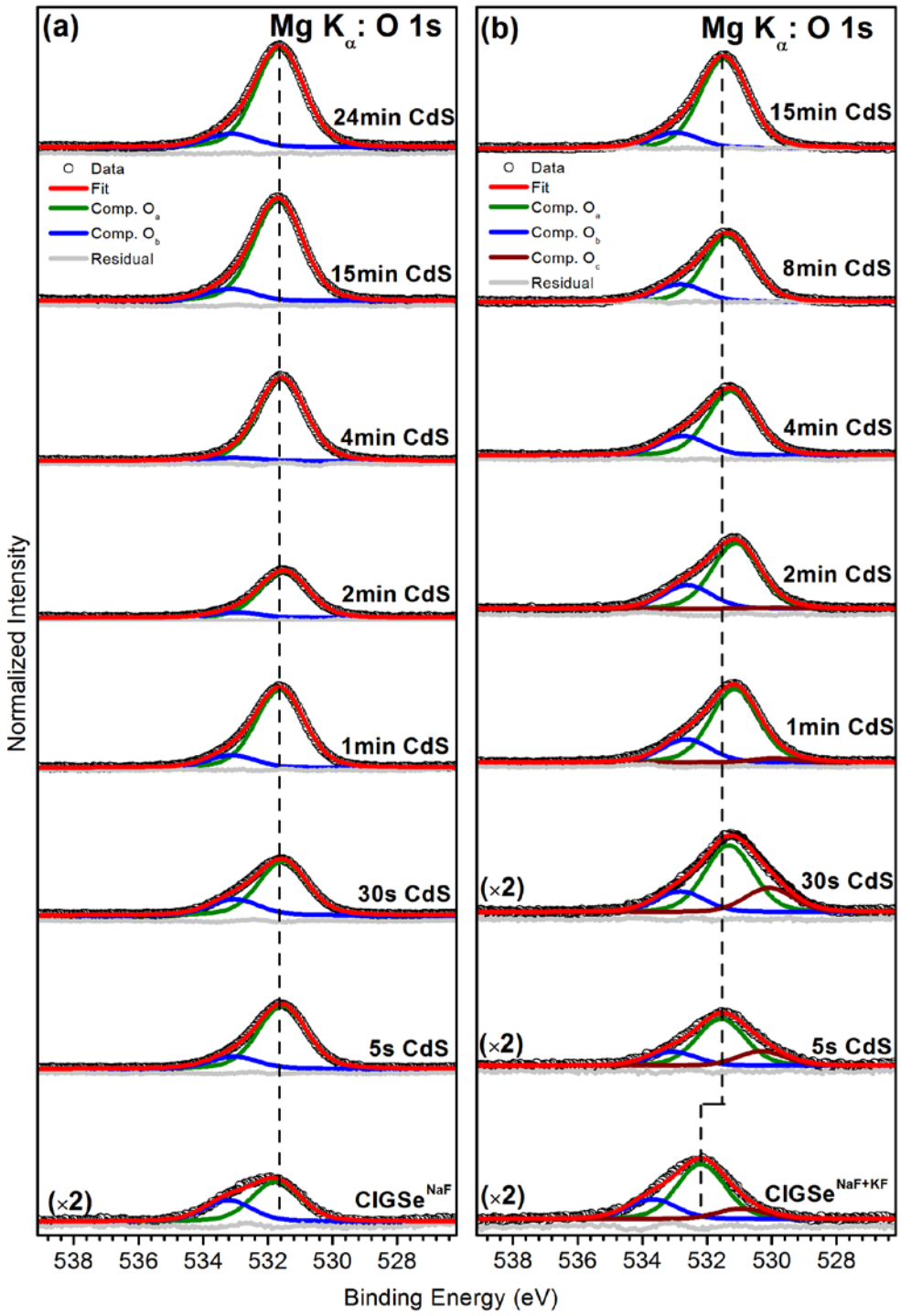

Figure S11. O 1s XPS data with respective Voigt fits of the CdS/CIGSe^{NaF} (a) and CdS/CIGSe^{NaF+KF} (b) sample series, measured with excitation energies of 1253.56 eV (Mg K$_\alpha$). All spectra are displayed after subtraction of a linear background. For each fit, the residual is shown as well. Note the different magnification factors. Spectra are vertically offset for clarity.

Figures S2-S11 show the detail spectra and corresponding fits of the background normalized Cu 3p, In 4d/Ga 3d, Se 3d, Na 1s (only for CdS/CIGSe^{NaF}), K 2p (only for CdS/CIGSe^{NaF+KF}), Cd 3d, Se 3s/S 2s, Cu 2p, In 3d, Ga 2p, and O 1s photoemission lines as a function of increasing

CBD time and for different PDT treatments. The Cu 3p spectra are shown after In 4p and Cd 4p background correction (see Figure S12-S15). As expected, most of absorber related signals decrease and the CdS buffer related signals increase in intensity with CBD time. All fits of a particular data set and for a particular photoemission line have been performed simultaneously using Voigt profiles with the same coupled Lorentz and Gauss widths. In case of spin-orbit doublet fits, the multiplicity rule (2j+1) is obeyed and the doublet separation for Cu 3p, In 4d, Ga 3d, Se 3d, and K 2p was set to 2.39 eV,[3] 0.86 eV,[4] 0.46 eV,[5] 0.83eV,[6] and 2.70 eV,[7] respectively. Note that the fit also included a linear background. Note that the Cd $3d_{3/2}$ and In $3d_{3/2}$ lines were chosen to fit instead of the more prominent respective $3d_{5/2}$ lines to avoid the Mg $K_{\alpha 3,4}$-excited $3d_{3/2}$ satellite lines that overlap with the $3d_{5/2}$ peak. All spectra but the O 1s line could be fit with one component. For O 1s more than one contribution (O_a and O_b for CdS/CIGSe^{NaF}; O_a, O_b, and O_c for CdS/CIGSe^{NaF+KF}) were needed for a satisfactory representation. Feature O_a at about 531.7 eV can be assigned to metal oxides [8-10], as e.g. In_2O_3,[8] Ga_2O_3,[9] or CdO.[10] Feature O_b located at 532.7 eV can be attributed to adsorbed hydroxyl species[11] and $Cd(OH)_2$[12]. The third component O_c between 530.0 and 530.8 eV which is only present in the data set of the CdS/CIGSe^{NaF+KF} series is attributed to potassium-oxygen bonds presumably with a mixed stoichiometry between K_2O and K_2O_2.[13] Note the small blue contribution to the Se 3s fit for the 1min CdS/CIGSe^{NaF} (Figure S7a) is attributed to a Mo 3d signal from the back contact presumably made accessible to the XPS analysis by accidental sample scratching during sample mounting. Furthermore, the broad signal detected at around 933 eV in Figure S8 for thicker CdS samples (i.e. ≥15 min for CdS/CIGSe^{NaF} and ≥2 min for CdS/CIGSe^{NaF+KF}) is ascribed to a Cd MNN plasmon background rather than to Cu $2p_{3/2}$.

All absorber layer related signals shift to lower binding energy for CdS/CIGSe^{NaF} sample series upon CdS deposition. The binding energy shift for CdS/CIGSe^{NaF+KF} series somewhat varies for every element, indicating a more complex situation.

3. Cu 3p background correction

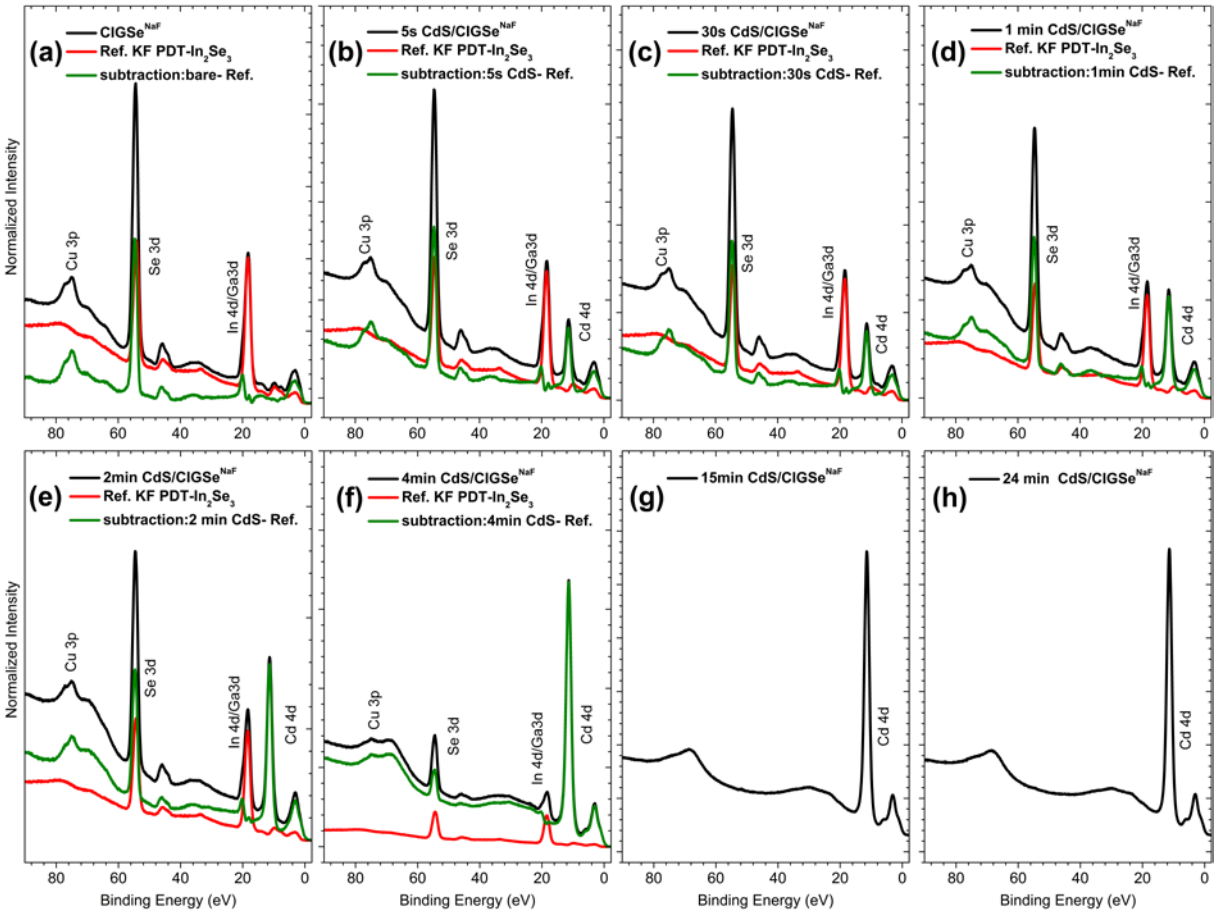

Figure S12. The In 4p background correction approach for the Cu 3p line using the respectively scaled and shifted In 4d line of the KF-PDT In_2Se_3 reference spectrum employed to the data set of the CdS/CIGSe^{NaF} sample series (CBD time: 0s (a), 5 s (b), 30 s, (c), 1 min (d), 2 min (e), 4 min (f) 15 min (g), and 24 min (h)), measured with an excitation energy of 1253.56 eV (Mg K_α). The as-measured spectra are shown in black, individually shifted and scaled references spectra in red, and the green spectra correspond to the resulting difference used for Cd 4p background.

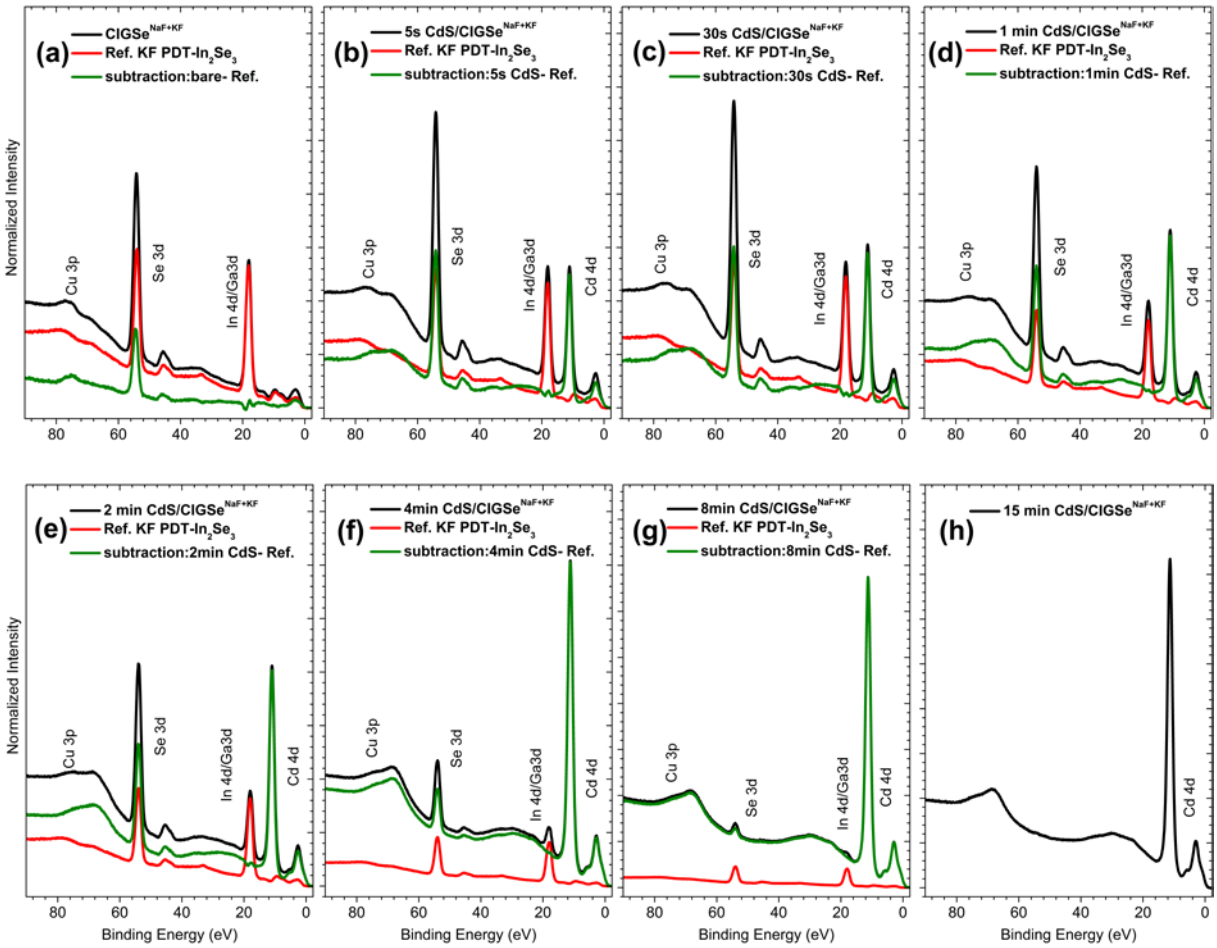

Figure S13. The In 4p background correction approach for the Cu 3p line using the respectively scaled and shifted In 4d line of the KF-PDT In_2Se_3 reference spectrum employed to the data set of the CdS/CIGSe^{NaF+KF} sample series (CBD time: 0s (a), 5 s (b), 30 s, (c), 1 min (d), 2 min (e), 4 min (f) 8 min (g), and 15 min (h)), measured with an excitation energy of 1253.56 eV (Mg K_α). The as-measured spectra are shown in black, individually shifted and scaled references spectra in red, and the green spectra correspond to the resulting difference used for Cd 4p background correction.

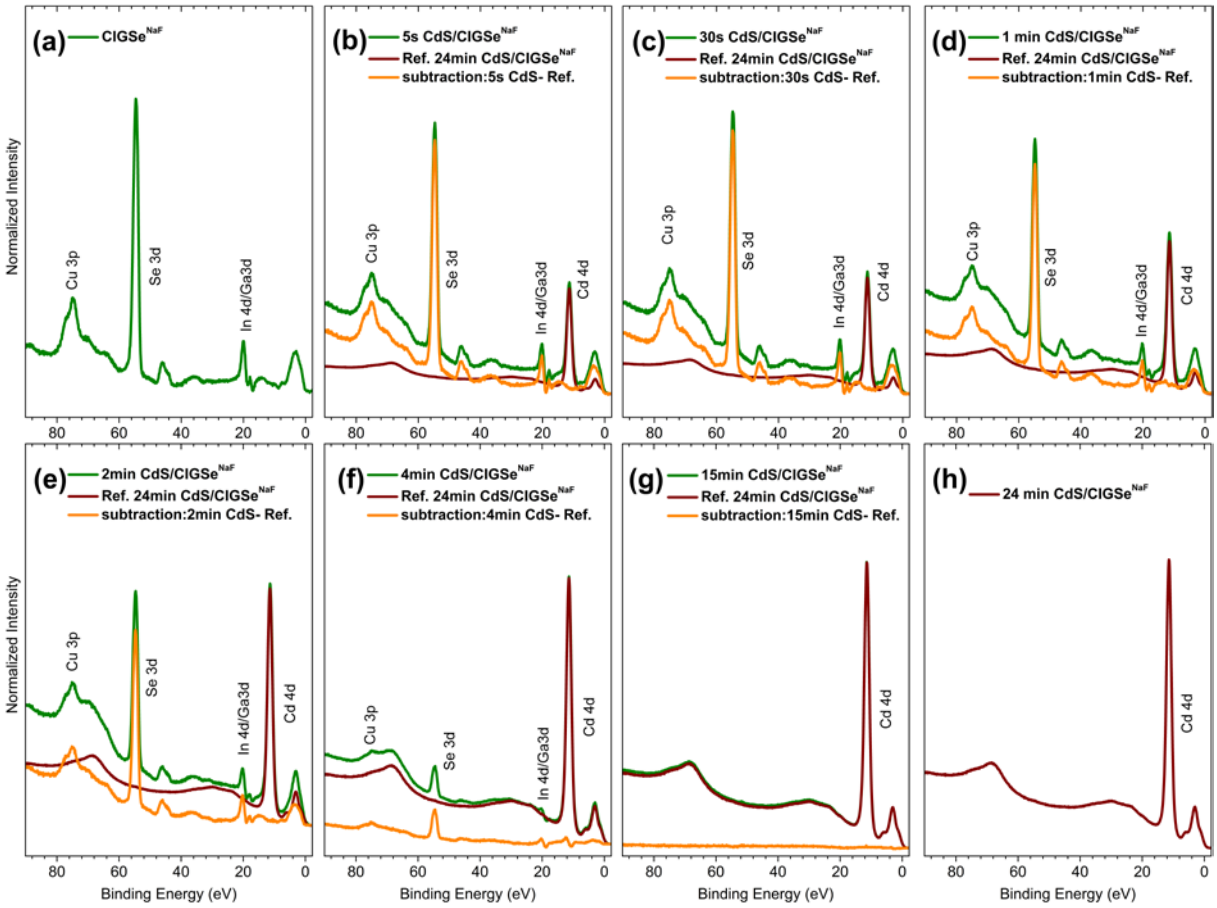

Figure S14. The Cd 4p background correction approach for the Cu 3p line using the respectively scaled and shifted Cd 4d line of the 24 min CdS/CIGSe^{NaF} sample employed to the whole data set (CBD time: 0s (a), 5 s (b), 30 s, (c), 1 min (d), 2 min (e), 4 min (f) 15 min (g), and 24 min (h)), measured with an excitation energy of 1253.56 eV (Mg K_α). The In 4p-corrected spectra are shown in green, individually shifted and scaled references spectra in wine, and the orange spectra correspond to the resulting difference used for further data evaluation.

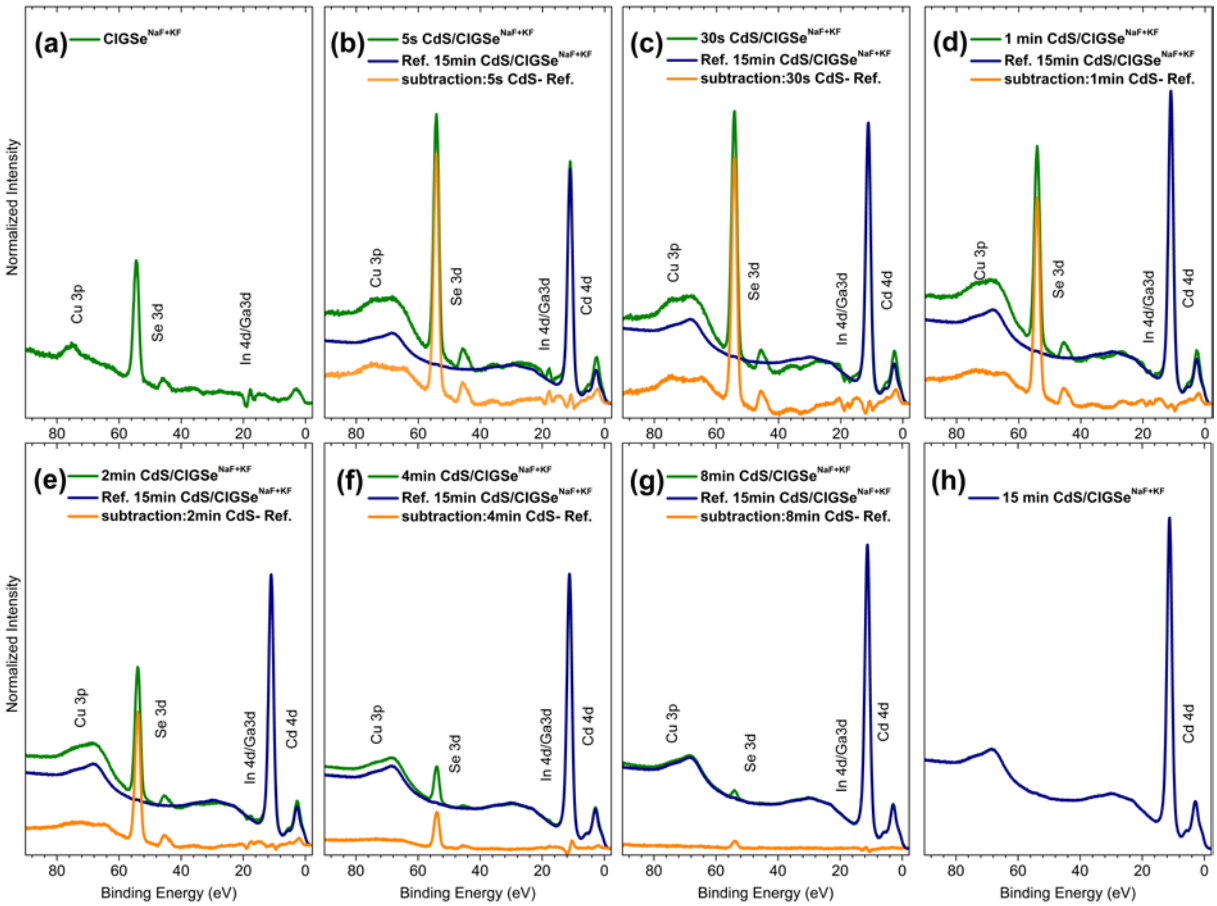

Figure S15. The Cd 4p background correction approach for the Cu 3p line using the respectively scaled and shifted Cd 4d line of the 15 min CdS/CIGSe^{NaF+KF} sample employed to the whole data set (CBD time: 0s (a), 5 s (b), 30 s, (c), 1 min (d), 2 min (e), 4 min (f) 8 min (g), and 15 min (h)), measured with an excitation energy of 1253.56 eV (Mg K_α). The In 4p-corrected spectra are shown in green, individually shifted and scaled references spectra in navy, and the orange spectra correspond to the resulting difference used for further data evaluation.

Figures S12-S15 visualize the Cu 3p background correction, subtracting (1) a properly shifted and scaled KF-PDT In_2Se_3 reference spectrum and (2) a properly shifted and scaled CdS reference spectrum (i.e., the spectrum of the thickest CdS sample of the respective sample series) to account for the broad In 4p and Cd 4p background (between 80 and 60 eV) that overlaps with the Cu 3p signal, respectively. For the proper energy shift and scaling factor for the reference spectra were derived by bringing the In 4d and Cd 4d lines, respectively, to maximum overlap. The “negative” overshoot in the range of the In 4d & Cd 4d line in the difference spectra can be explained by different composition profiles and/or slight variations of the core level binding energies.

4. Thickness calculation

The evolution of the intensity (mainly attenuation) of the absorber-related lines with CBD-CdS treatment periods is used to estimate the effective thickness of the attenuating buffer layers.

Based on the fitting results of the (shallow) core level spectra (Figures S2-S7), the buffer layer thickness is calculated based on the inelastic mean free path (IMFP) of the respective photoelectrons in CdS.[14] For absorber layer related elements, the intensity I^{abs} attenuated due to the increasing buffer layer and the effective buffer layer thickness d^{buf} are related – considering the used measurement geometry – according to the following formula:

$$I^{abs} = I_0 \times e^{-\frac{d^{buf}}{IMFP}} \quad (1)$$

where I_0 is the intensity of the lines of the bare CIGSe substrate. Note for this approach it is assumed that the buffer grows homogenously layer-by-layer.

Similarly, for buffer layer related elements, the effective buffer thickness d^{buf} and the intensity of the increasing buffer-related photoemission lines I^{buf} are related according to:

$$I^{buf} = I_1 \times (1 - e^{-\frac{d^{buf}}{IMFP}}) \quad (2)$$

Here I_1 is the intensity of the buffer-related photoemission lines for the thickest buffer layer (i.e., 24 min CdS/CIGS^{NaF} and 15 min CdS/CIGS^{NaF+KF}). The used IMFP values (in CdS) for the respective core level photoelectrons are shown in Table S1.

Table S1. Calculated inelastic mean free path for the different photoelectrons in CdS according to the TPP2M formula.[14]

Photoelectrons (excited with Mg K_α)	Inelastic mean free path [nm]
Cu 3p (E_K =1173.6 eV)	2.233
In 4d (E_K =1236.6 eV)	2.325
Ga 3d (E_K =1233.6eV)	2.321
Se 3d (E_K =1193.6 eV)	2.262
Cd 3d (E_K =838.6 eV)	1.738
S 2s (E_K =1023.6 eV)	2.008
Na 1s (E_K =178.6 eV)	0.642
K 2p (E_K =957.6 eV)	1.933

5. Se $M_{4,5}$: Area-normalized presentation & fit procedure

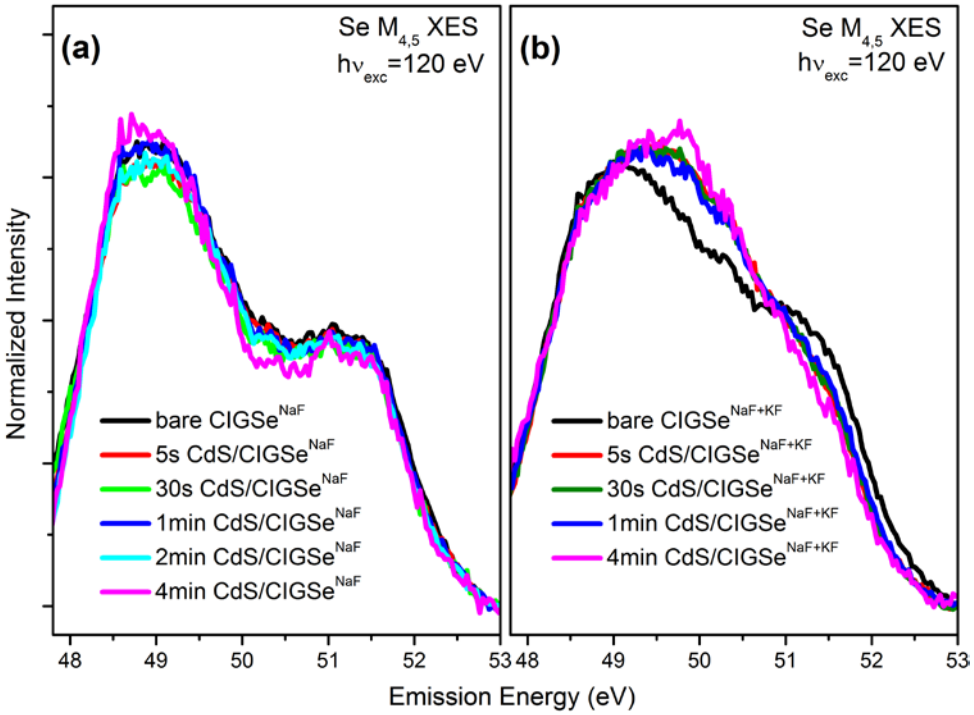

Figure S16. Area normalized Se $M_{4,5}$ XES spectra of the CdS/$CIGSe^{NaF}$ (a) and CdS/$CIGSe^{NaF+KF}$ (b) sample series.

The Se $M_{4,5}$ XES spectra of the CdS/$CIGSe^{NaF+KF}$ sample set are represented by the sum of different reference spectra as shown in Figure S17 and S18. Figure S17 a and S18 a show the weighted sum of the spectrum of the $CIGSe^{NaF}$ sample and that of the KF-PDT In_2Se_3 reference exactly representing the spectrum of the $CIGSe^{NaF+KF}$ sample. This is an indication for the formation of a K-In-Se type species as a result of a NaF+KF PDT, corroborating previous results.[15] The representation of the spectra of the CdS/$CIGSe^{NaF+KF}$ samples by the weighted sum of the spectrum of the bare $CIGSe^{NaF}$ sample and that that of a CdSe reference is displayed in Figure S17 b-f. Figures S18 b-f show the representation of the same data set by the weighted sum of the spectrum of the bare $CIGSe^{NaF+KF}$ sample and (again) that of a CdSe reference. The quantified values of the different spectral contributions are stated in the Figures, the uncertainty of these values is around ±0.03. The absolute area of the spectral residuals is also shown in the Figures above as a measure of the goodness of the fit. Apparently, the applied fit models (i.e., $CIGSe^{NaF}$ + CdSe and $CIGSe^{NaF+KF}$ + CdSe) result in similarly good fits.

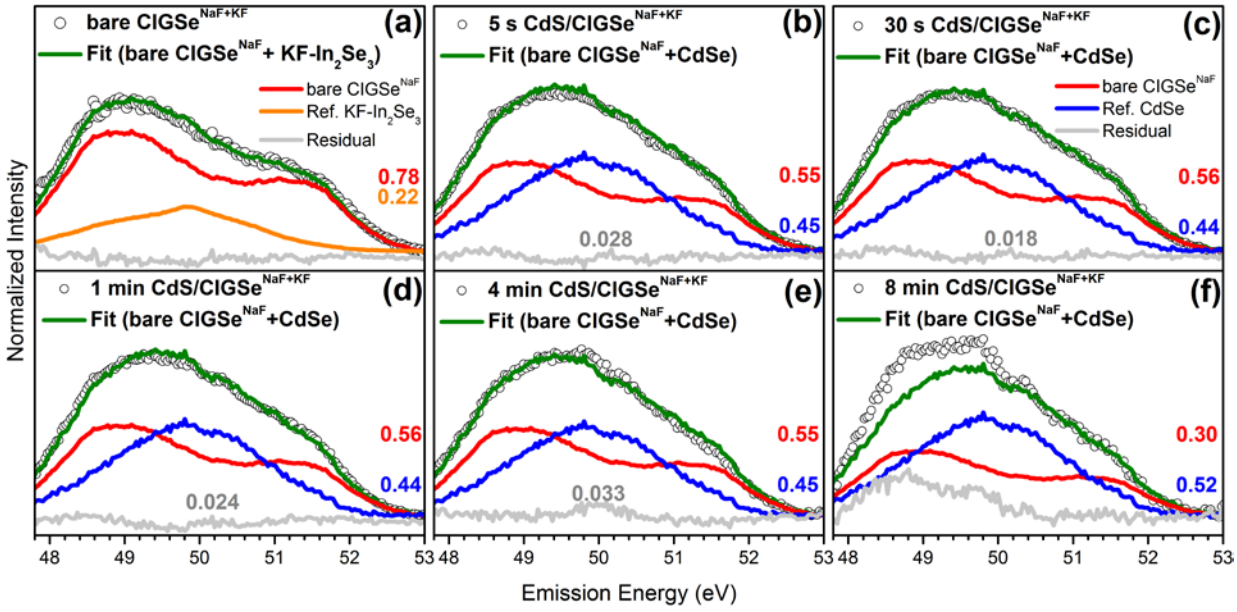

Figure S17. Se $M_{4,5}$ XES spectra of the CdS/CIGSe^{NaF+KF} sample set (CBD time: 0s (a), 5 s (b), 30 s, (c), 1 min (d), 4 min (e), and 8 min (f)) represented by a spectral sum (green) of the spectra of CIGSe^{NaF} (red), KF-PDT In_2Se_3 (orange) and CdSe (blue). The quantified values for the spectral contributions and the residuals are also shown. Furthermore, the absolute area of the spectral residuals is stated as measure for the goodness of the fit.

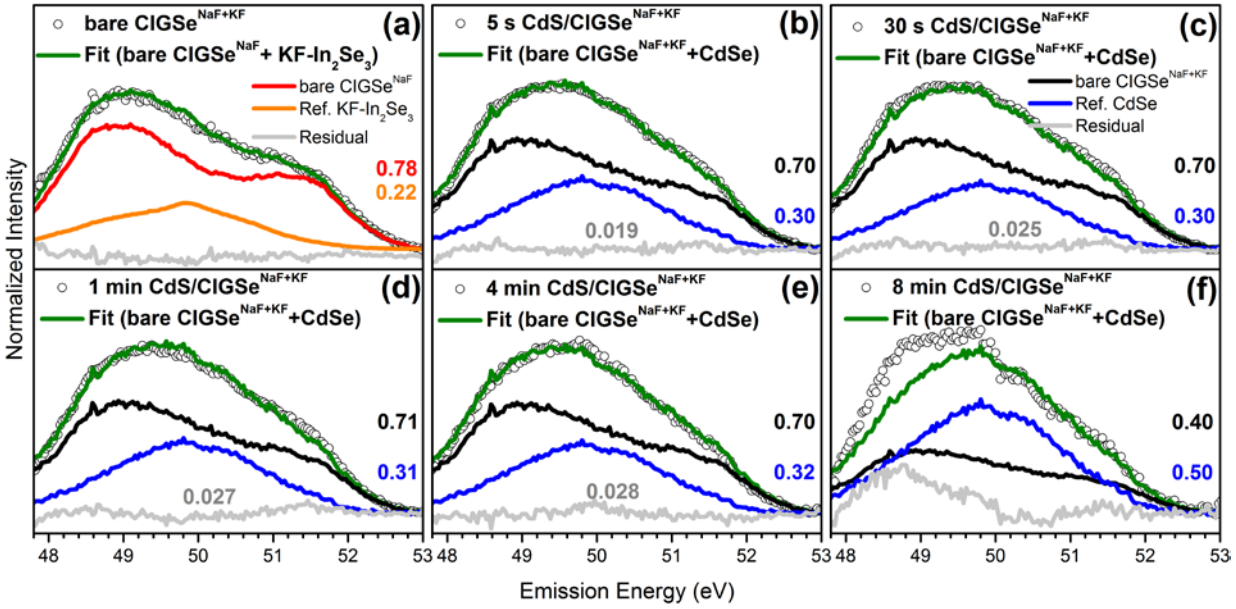

Figure S18. The Se $M_{4,5}$ XES spectrum of the CIGSe^{NaF+KF} sample (a) is represented by a spectral sum (green) of the spectra of CIGSe^{NaF} (red) and KF-PDT In_2Se_3 (orange) as shown in Figure S17a. The Se $M_{4,5}$ XES spectra of the CdS/CIGSe^{NaF+KF} sample set (CBD time: 5 s (b), 30 s, (c), 1 min (d), 4 min (e), and 8 min (f)) is represented by a spectral sum (green) of the spectra of CIGSe^{NaF+KF} (black) and CdSe (blue). The quantified values for the spectral contributions and the residuals are also shown. Furthermore, the absolute area of the spectral residuals is stated as measure for the goodness of the fit.

6. Comparison of K 2p and O 1s-related contributions

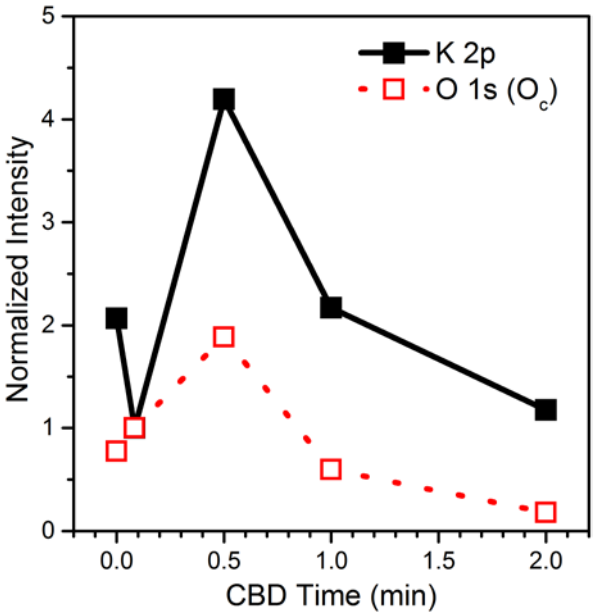

Figure S19. Intensity evolution of the K 2p (black) and O_c species (red) with increasing CBD time, normalized to the respective intensity values derived for the 5s CdS/CIGSe^{NaF+KF} sample.

As shown in Figure S11, there is a clear difference between the O 1s spectra of the CdS/CIGSe sample sets. In the CdS/CIGSe^{NaF+KF} series, an additional low-binding energy O 1s component (O_c) appears for CBD times ≤ 2 min. In the same CBD regime, we find a clear K 2p signal (Figure S5b) on the respective samples. Comparing the intensity evolution of the K $2p_{3/2}$ peak to that of the O 1s feature O_c in Figure S19, a clear correlation is revealed for CBD times ≥ 5s suggesting the presence of O-K bonds (see also discussion in conjunction to Figure S5b, above). The deviation for the bare absorber can be explained by potassium being present in a different chemical environment (→ K-In-Se type species). The significant intensity variation of the K 2p (and the O 1s (O_c)) line in the early stages of the CBD process indicates a complicated process involving dissolution and redeposition, or possibly diffusion. Furthermore, it should be considered that the formation of K-O bonds in this CBD time regime could very well be an artifact of sample preparation (i.e., retrieving the samples after the given time in the CBD solution with subsequent rinsing).

7. Cd MNN spectra: Background correction and fit

Since the Cd $M_{45}N_{45}N_{45}$ spectra (E_K: 370 eV~390eV) are significantly influenced by the In $M_{45}N_{45}N_{45}$ (E_K: 395 eV~415eV) spectra, In $M_{45}N_{45}N_{45}$ spectra were subtracted according to the fitting results depicted in Figure 3. The subtraction details are visualized in Figure S20.

After In $M_{45}N_{45}N_{45}$ background correction, peak-area-normalized Cd $M_4N_{45}N_{45}$ spectra were fitted, shown in Figure S21. Since Cd MNN Auger spectra of the thickest samples for each data set (i.e. the spectrum of the 24 min CdS/CIGSe^{NaF} sample and the spectrum of the 15 min CdS/CIGSe^{NaF+KF} sample) have the same spectral shape and are the narrowest, these spectra were also used as single-species references to (properly scaled and shifted) fit all other Cd MNN Auger spectra.

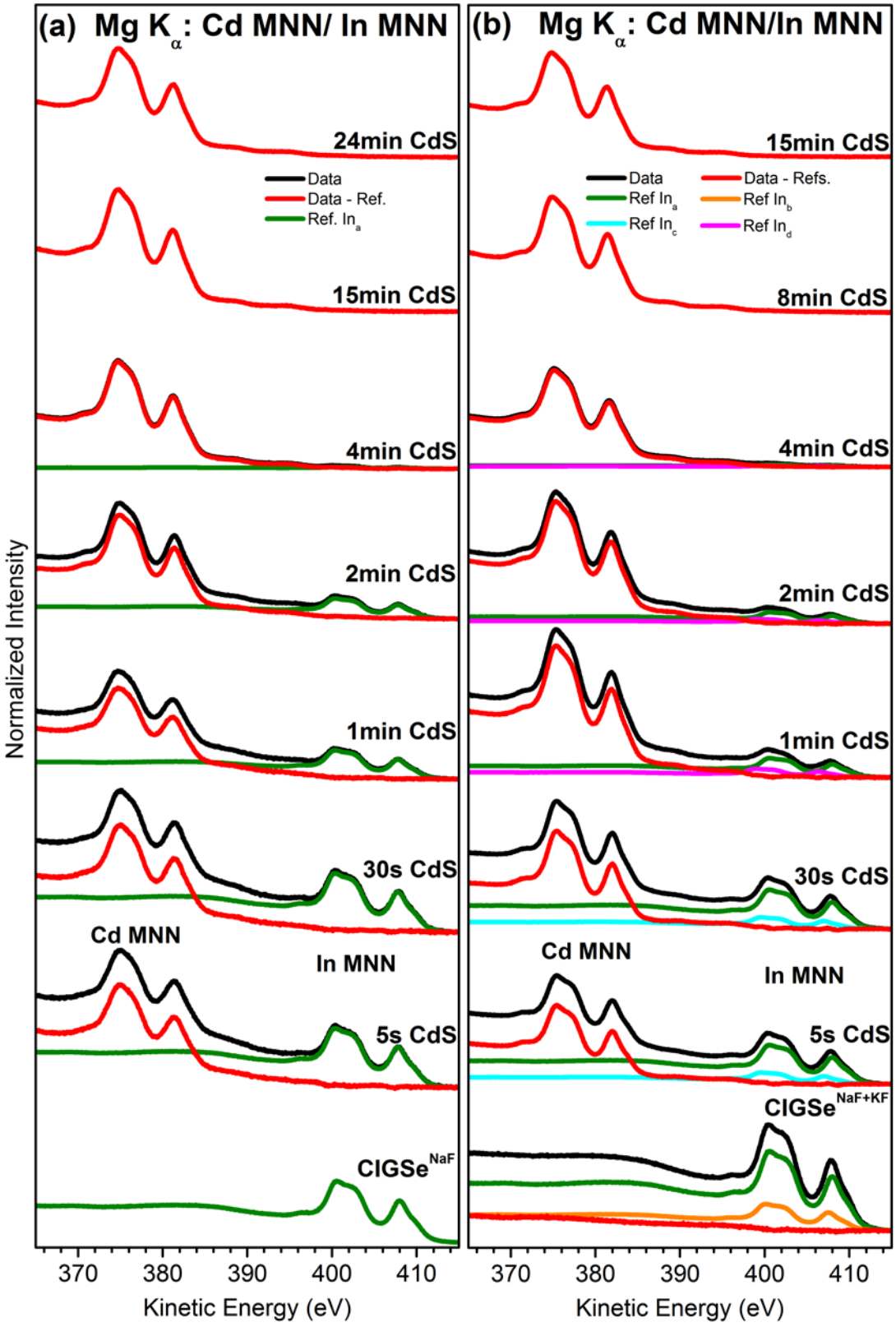

Figure S20. The In MNN background subtraction of the Cd MNN lines according to the fitting results in Figure 3 for the data set of the CdS/CIGSe^{NaF} (a) and CdS/CIGSe^{NaF+KF} (b) sample series, measured with an excitation energy of 1253.56 eV (Mg K$_\alpha$). The as-measured spectra are shown in black, individually shifted and scaled references spectra are depicted in green/orange/cyan/ magenta, and the red spectra represent to the background corrected Cd MNN Auger spectra. Spectra are vertically offset for clarity.

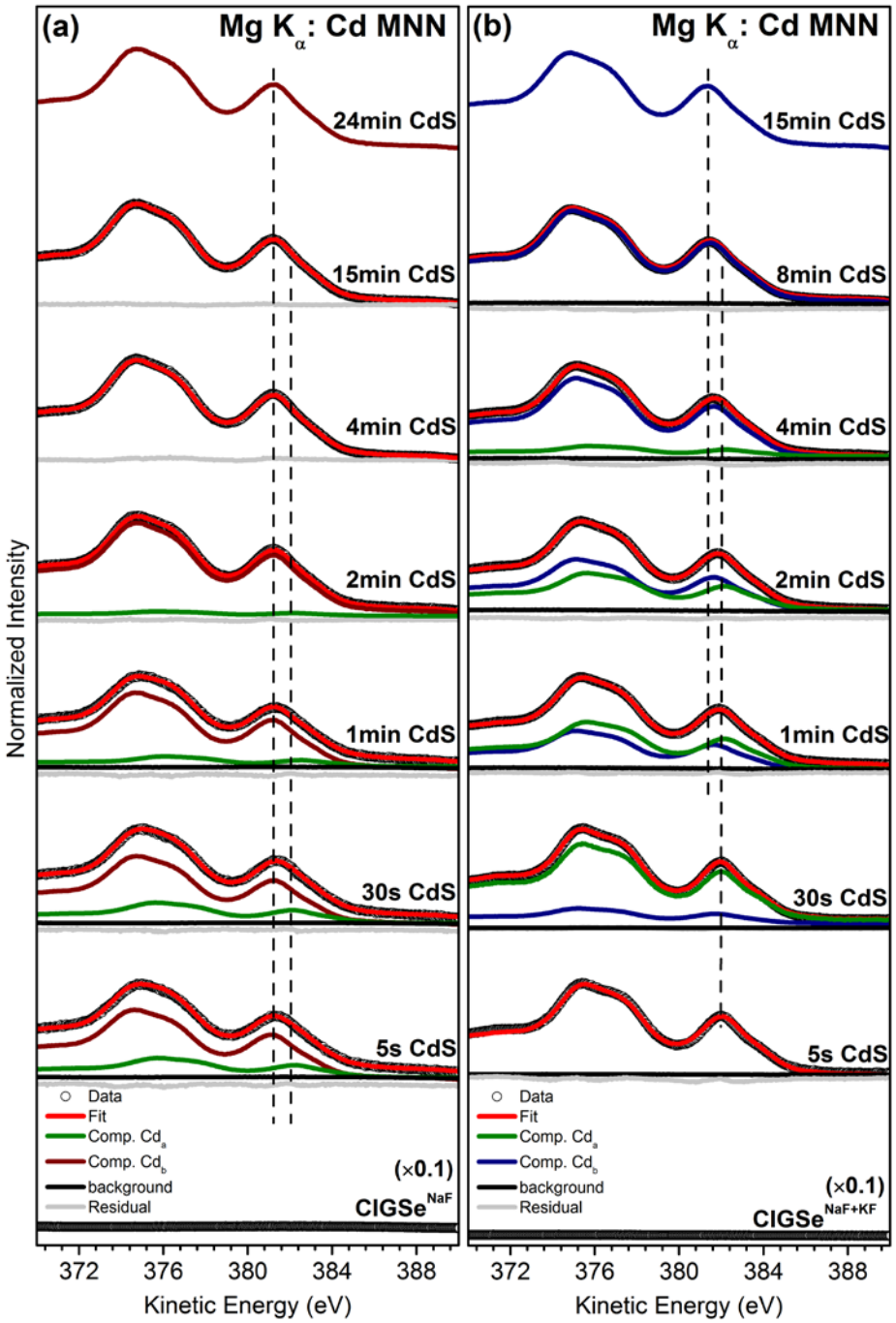

Figure S21. In MNN background-corrected Cd $M_{45}N_{45}N_{45}$ XAES lines of the CdS/CIGSe^{NaF} (a) and CdS/ PDT/CIGSe^{NaF+KF} (b) sample series with increasing CBD time, measured using Mg K_α excitation. Vertical offsets are added for clarity. The reference spectra representing component Cd_a or Cd_b are properly scaled and shifted Cd MNN spectra of the thickest sample per sample set (i.e., the spectrum of the 24 min CdS/CIGSe^{NaF} sample and that of the 15 min CdS/CIGSe^{NaF+KF} sample are used as single-species references).

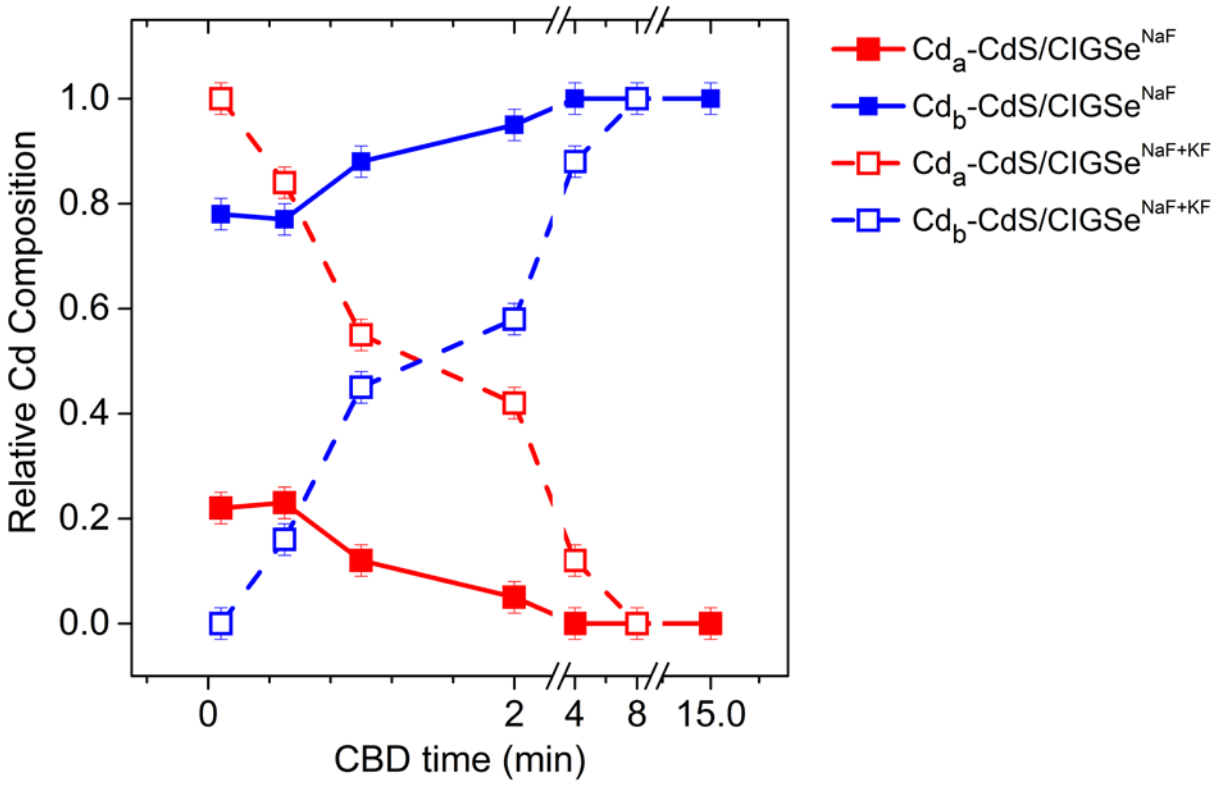

Figure S22. Relative Cd compound compositions of the CdS/CIGSe^{NaF} (solid square) and CdS/CIGSe^{NaF+KF} (open square) sample sets with increasing CBD time according to the Cd MNN fit results in Figure S21.

8. Definition of reference boxes for the comparison to derived modifed Auger parameters for In and Cd

In order to use the derived modified Auger parameters of In and Cd to identify different compounds, we ought to compare with reference values. However, there is only a very limited amount of modified Auger parameter values reported in literature. Thus, we constructed reference boxes that are based on the reported (very common) binding energy values for In 3d or Cd 3d and the reported kinetic energies of the corresponding MNN Auger line for a specific compound; when combined these values represent the largest possible spread of modified Auger parameters. In the following you will find a summary of the used binding and kinetic energy values used:

In previous reports, the In MNN Auger kinetic energies of In_2Se_3 are located between 408.0 - 408.3 eV.[16-17] Corresponding In $3d_{5/2}$ binding energies can be found between 444.3 and 445.1 eV.[16-18] Similarly, for $CuInSe_2$ we find 408.4 eV [18] and 443.9 eV[16] - 445 eV[19]; for $CuIn_3Se_5$ we find 407.4 eV [17] and 444.1 eV - 444.8 eV [16-17]; for In_2S_3 we find 407.3 - 407.4 eV [17, 20] and 444.7 - 445 eV[17, 20-21]; for In_2O_3 we find 406.0 - 406.8 eV [22-23] and 444.4 - 445 eV [18, 24]. Note that the doublet separation between In $3d_{3/2}$ (used in the analysis) and In $3d_{5/2}$ (for which reference values are reported) is 7.54 eV[25] and was considered when computing the modified Auger parameters derived from the measured data.

For the Cd modified Auger parameter, we followed a similar procedure. We combined the following kinetic energies of Cd MNN Auger and corresponding binding energies of Cd $3d_{5/2}$ peaks: for CdSe 381.20 eV – 381.90 eV [26-27] and 404.80 - 405.45 eV [17, 27-28]; for CdS 381.00 – 381.6 eV [17, 29] and 405.00 – 405.40 eV [30-31]; for $Cd(OH)_2$ 379.90 – 380.7 [29, 32] and 405.10 - 405.60 eV [32-34]; for CdO 382.1 - 382.7 eV [29, 34-35] and 404.00 – 405.2 eV.[17, 34-35]. Note that also in this case the doublet separation between Cd $3d_{5/2}$ and Cd $3d_{3/2}$ of 6.75 eV[36] has to be considered for the measured data.

9. The Cd/anion ratio of the deposited buffer layer

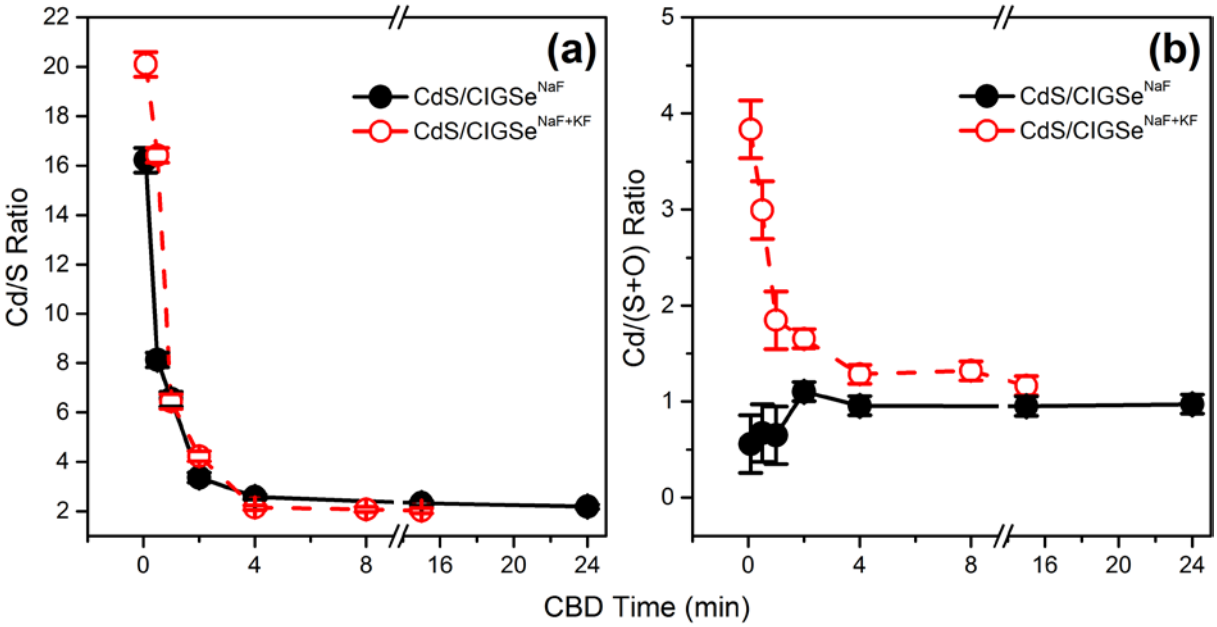

Figure S23. Evolution of (a) the Cd/S ratio and (b) the Cd/(S+O_{a+b}) ratio with increasing CBD time. The ratios were derived based on the fit results in Figures S6, S7, and S11, corrected by the respective inelastic mean free path (IMFP calculated by TPP2M[14]), analyzer transmission function, and photoionization cross section values.[37]

10. S $L_{2,3}$ XES: Direct comparison of CdS/CIGSe samples prepared in different temperature regimes

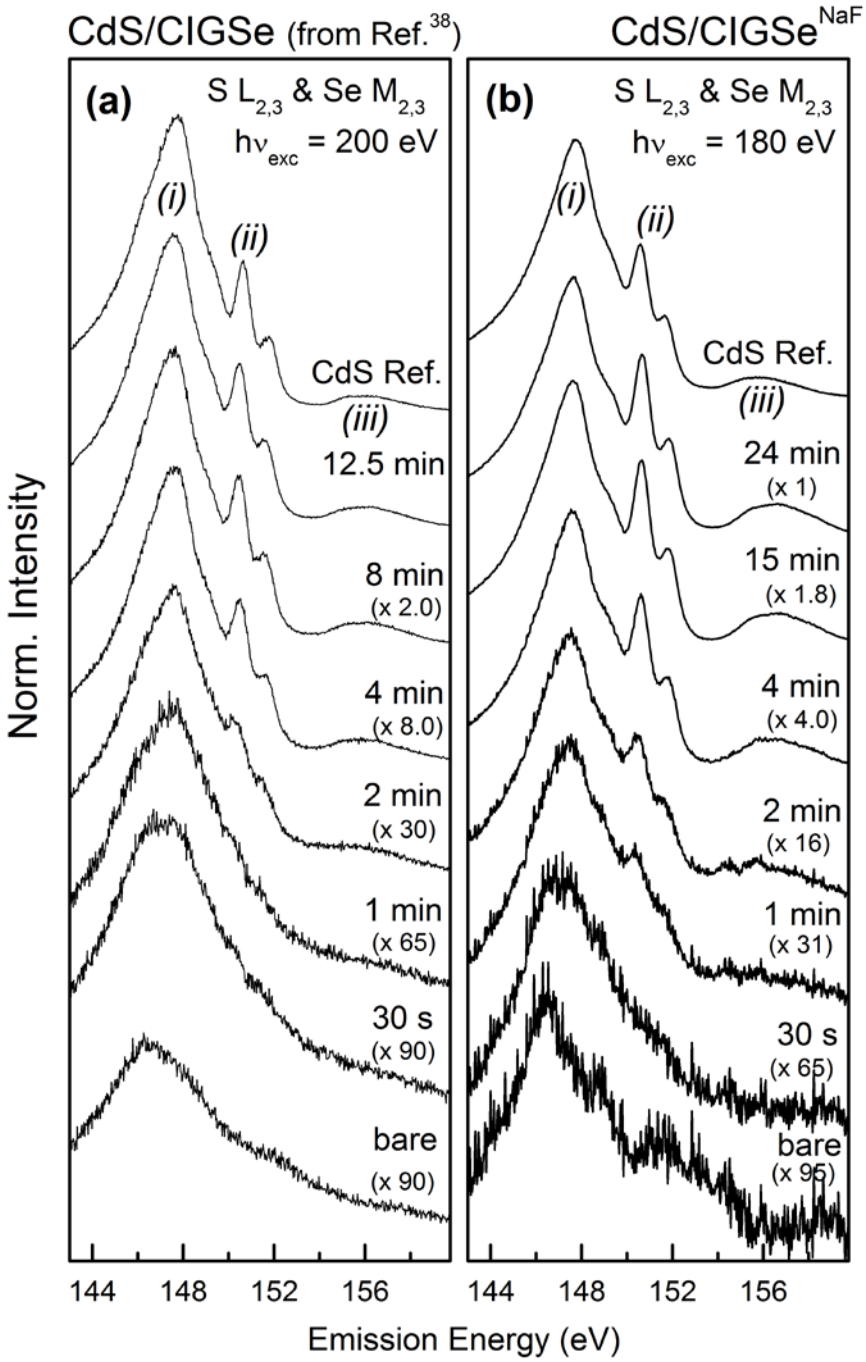

Figure S24. S $L_{2,3}$/Se $M_{2,3}$ XES spectra of K-free CdS/CIGSe samples as a function of CBD time prepared based on high-temperature processed ((a), Reproduced with permission from reference [38]. Copyright 2010 American Institute of Physics) and low-temperature processed ((b), compare to Figure 6a of this study) CIGSe absorber. The main features are labeled (i)−(iii). Spectra are normalized to equal peak height above background and vertically offset for clarity. Note the different magnification factors.

In order to compare the findings related to the chemical structure of the (buried) CdS/CIGSe^{NaF} with reports in literature, Figure S24 shows a direct comparison of the S $L_{2,3}$/Se $M_{2,3}$ XES

spectra to previously measured XES data of a similar CdS/CIGSe sample set (from Ref.[38]). The main difference in the sample sets is the fact that the absorbers of the different series were prepared in different temperature regimes. While the absorbers of this study have been prepared at low temperatures (to facilitate the employment of flexible polyimide type substrates), the absorber used in the previous study was deposited at higher temperatures. In addition, for the low temperature processed CIGSe absorber of the current study a PDT was performed, while for the high temperature processed absorbers of the previous study one relied on the diffusion from the soda-lime glass as the sole sodium source. Nevertheless, at first sight, the spectra look very similar. The main features are associated with[39] (i) S 3s states, (ii) Cd 4d-derived bands (i.e., Cd 4d → S $2p_{3/2}$, and Cd 4d → S $2p_{1/2}$ transitions, respectively), and (iii) the upper valence band (UVB). However close inspection of the spectra, in particular those that represent samples with buffer layers that have been deposited within short (i.e., 1 and 2 min) CBD times, reveals that the Cd 4d-derived features are differently pronounced. In the old data sat, the Cd 4d-derived features are (almost) completely missing (for the 1 min CdS/CIGSe sample) and significantly reduced in intensity (for the 2 min CdS/CIGSe sample) compared to the spectra of the respective CdS/CIGSe^{NaF} samples of this study. Previously, the apparent presence of S-related spectral intensity without the presence of the Cd 4d-derived features was interpreted as a CBD-CdS process induced S-deposition without the deposition of Cd / the formation of S-Cd bonds. In this particular case, it was concluded that an $(In_{1-x}Ga_x)_yS_z$ type interface layers between CdS and the CIGSe absorber is formed.[38]

In the current case, we can clearly identify Cd 4d-derived features in the spectrum of the 1 min CdS/CIGSe^{NaF} sample, which indicates a significantly reduced induction period of the CBD-CdS process may be caused by a different surface structure of the low temperature processed and PDTed CIGSe absorber.

References

(1) Hüfner, S. *Photoelectron Spectroscopy: Principles and Applications*, Springer: 2013.

(2) Bär, M.; Weinhardt, L.; Heske, C. Soft X‐ray and Electron Spectroscopy: A Unique "Tool Chest" to Characterize the Chemical and Electronic Properties of Surfaces and Interfaces. In *Advanced Characterization Techniques for Thin Film Solar Cells*; Abou‐Ras, D. K., T.; Rau. U., Ed.; Wiley-VCH: Weinmheim, Germany, 2016.

(3) Lebugle, A.; Axelsson, U.; Nyholm, R.; Martensson, N. Experimental L and M Core Level Binding Energies for the Metals ^{22}Ti to ^{30}Zn. *Phys. Scr.* **1981,** *23*, 825-827.

(4) Poole, R. T.; Kemeny, P. C.; Liesegang, J.; Jenkin, J. G.; Leckey, R. C. G. High Resolution Photoelectron Studies of the d Bands of Some Metals. *J. Phys. F: Metal Phys.* **1973,** *3*, L46-L48.

(5) Poirier, D. M.; Weaver, J. H. GaAs(110) by XPS. *Surface Science Spectra* **1993,** *2*, 201-208.

(6) Shevchik, N. J.; Cardona, M.; Tejeda, J. X-Ray and Far-uv Photoemission from Amorphous and Crystalline of Se and Te. *Phys. Rev. B* **1973,** *8*, 2833-2841.

(7) Petersson, L. G.; Karlsson, S. E. Clean and Oxygen Exposed Potassium Studied by Photoelectron Spectroscopy. *Phys. Scr.* **1977,** *16*, 425-431.

(8) Sutter, E. A.; Tong, X.; Jungjohann, K.; Sutter, P. W. Oxidation of Nanoscale Au–In Alloy Particles as A Possible Route Toward Stable Au-Based Catalysts. *PNAS* **2013,** *110*, 10519.

(9) Shalish, I.; Shapira, Y.; Burstein, L.; Salzman, J. Surface States and Surface Oxide in GaN Layers. *J. Appl. Phys.* **2001,** *89*, 390-394.

(10) Eom, N. S. A.; Kim, T. S.; Choa, Y. H.; Kim, W. B.; Kim, B. S. Surface Oxidation Behaviors of Cd-Rich CdSe Quantum Dot Phosphors at High Temperature. *J. Nanosci. Nanotechnol.* **2014,** *14*, 8024-8027.

(11) Brown, M. A.; Fujimori, Y.; Ringleb, F.; Shao, X.; Stavale, F.; Nilius, N.; Sterrer, M.; Freund, H.-J. Oxidation of Au by Surface OH: Nucleation and Electronic Structure of Gold on Hydroxylated MgO(001). *J. Am. Chem. Soc.* **2011,** *133*, 10668-10676.

(12) Kishi, K.; Ikeda, S. X-Ray Photoelectron Spectroscopic Study for the Reaction of Evaporated Iron with O_2 and H_2O. *Bull. Chem. Soc. Jpn.* **1973,** *46*, 341-345.

(13) Kim, M. G.; Kanatzidis, M. G.; Facchetti, A.; Marks, T. J. Low-Temperature Fabrication of High-Performance Metal Oxide Thin-Film Electronics via Combustion Processing. *Nat. Mater.* **2011,** *10*, 382-388.

(14) Tanuma, S.; Powell, C. J.; Penn, D. R. Calculations of Electron Inelastic Mean Free Paths. *Surf. Interface Anal.* **1993,** *20*, 77-89.

(15) Handick, E.; Reinhard, P.; Wilks, R. G.; Pianezzi, F.; Kunze, T.; Lorenzo, D. K.; Weinhardt, L.; Blum, M.; Yang, W.; Gorgoi, M.; Ikenaga, E.; Gerlach, D.; Ueda, S.; Yamashita, Y.;Chikyow, T.; Heske, C.; Buecheler, S.; Tiwari, A. N.; Bär, M. Formation of a K-In-Se Surface Species by NaF/KF PostdepositionTreatment of Cu(In,Ga)Se_2 Thin-Film Solar Cell Absorbers. *ACS Appl. Mater. Interfaces* **2017,** *9*, 3581-3589.

(16) Cahen, D.; Ireland, P. J.; Kazmerski, L. L.; Thiele, F. A. X-ray Photoelectron and Auger Electron Spectroscopic Analysis of Surface Treatments and Electrochemical Decomposition of $CuInSe_2$ Photoelectrodes. *J. Appl. Phys.* **1985,** *57* (10), 4761-4771.

(17) Moulder, J. F.; Stickle, W. F.; Sobol, P. E.; Bomben, K. D. *Handbook of X-Ray Photoelectron Spectroscopy*, Minnesota, USA, 1995.

(18) Kazmerski L. L.; Jamjoum O.; Ireland P. J.; Deb, S. K. R.; Mickelsen A.; Chen W. Initial Oxidation of $CuInSe_2$. *J. Vacuum Sci. & Technol.* **1981,** *19*, 467-471.

(19) Von Morzé, N.; Dittrich, T.; Calvet, W.; Lauermann, I.; Rusu M. Transient and Modulated Charge Separation at $CuInSe_2$/C60 and $CuInSe_2$/ZnPc Hybrid Interfaces. *Appl. Surf. Sci.* **2017,** *396*, 366-374.
(20) Sterner, J.; Malmström, J.; Stolt, L. Study on ALD In_2S_3/Cu(In,Ga)Se_2 Interface Formation. *Prog. Photovolt. Res. Appl.* **2005,** *13*, 179-193.
(21) Briggs, D.; Seah, M. P. *Practical Surface Analysis: Auger and X-ray Photoelectron Spectroscopy*, Wiley: New York 1983.
(22) Faur, M.; Jayne, D. T.; Goradia, M.; Goradia, C. XPS Investigation of Anodic Oxides Grown on P-type InP. *Surf. Interface Anal.* **1990,** *15*, 641-650.
(23) Lin, A. W. C.; Armstrong N. R.; Kuwana, T. X-ray Photoelectron/Auger Electron Spectroscopic Studies of Tin and Indium Metal Foils and Oxides. *Ana. Chem.* **1977,** *49*, 1228-1235.
(24) Bertrand, P. A. XPS Study of Chemically Etched GaAs and InP. *J. Vacuum Sci. & Technol.* **1981,** *18*, 28-33.
(25) Dai, M. Z.; Khan, K.; Zhang, S. N.; Jiang, K. J.; Zhang, X. Y.; Wang, W. L.; Liang, L. Y.; Cao, H. T.; Wang, P. J.; Wang, P.; Miao, L. J.; Qin, H. M.; Jiang, J.; Xue, L. X.; Chu, J. H. A Direct Method to Extract Transient Sub-Gap Density of State (DOS) Based on Dual Gate Pulse Spectroscopy. *Sci. Rep.* **2016,** *6*, 24096.
(26) Islam, R.; Rao, D. R. X-ray Photoelectron Spectroscopy of $Zn_{1-x}Cd_xSe$ Thin Films. *J. Electron. Spectrosc. Relat. Phenom.* **1996,** *81*, 69-77.
(27) Polak, M. X-Ray Photoelectron Spectroscopic Studies of $CdSe_{0.65}Te_{0.35}$. *J. Electron. Spectrosc. Relat. Phenom.* **1982,** *28*, 171-176.
(28) Banerjeea, S.; Wong, S. S. Formation of CdSe Nanocrystals onto Oxidized, Ozonized Single-Walled Carbon Nanotube Surfaces. *ChemComm* **2004**, 1866-1867.
(29) Niles, D. W.; Herdt, G.; Al-Jassim, M. An X-ray Photoelectron Spectroscopy Investigation of O Impurity Chemistry in CdS Thin Films Grown by Chemical Bath Deposition. *J. Appl. Phys.* **1997,** *81*, 1978-1984.
(30) Bhide, V. G.; Salkalachen, S.; Rastog, A. C.; Rao, C. N. R.; Hegde, M. S. Depth Profile Composition Studies of Thin Film CdS:Cu_2S Solar Cells Using XPS and AES. *J. Phys. D: Appl. Phys.* **1981,** *14*, 1647-1656.
(31) Riga, J.; Verbist, J. J.; Josseaux, P.; Mesmaeker, A. K. Correlation between CdS Photoanodic Behaviour and Electrode Chemical Modifications: An X‐ray Photoelectron Spectroscopic Study. *Surf. Interface Anal.* **1985,** *7*, 163-168.
(32) Wagner C.D.; Gale L. H.; Raymond, R. H. Two-Dimensional Chemical State Plots: A Standardized Data Set for Use in Identifying Chemical States by X-ray Photoelectron Spectroscopy. *Ana. Chem.* **1979,** *51*, 466-482.
(33) Zhang, D. E.; Pan, X. D.; Zhu, H.; Li, S. Z.; Xu, G. Y.; Zhang, X. B.; Ying, A. L.; Tong, Z. W. A Simple Method to Synthesize Cadmium Hydroxide Nanobelts. *Nanoscale Res. Lett.* **2008,** *3* (8), 284-288.
(34) Tkachenko, O. P.; Shpiro, E. S.; Wark, M.; Ekloff, G. S.; Jaeger, N. X-Ray Photoelectron/X-Ray Excited Auger Electron Spectroscopic Study of Highly Dispersed Semiconductor CdS and CdO Species in Zeolites. *J. Chem. Soc. Faraday Trans.* **1993,** *89*, 3987-3994.
(35) Gaarenstroom, S. W.; Winograd, N. Initial and Final State Effects in the ESCA Spectra of Cadmium and Silver Oxides. *J. Chem. Phys.* **1977,** *67*, 3500-3506.
(36) White, H. S.; Rlcco, A. J.; Wrighton, M. S. Characterization of p-Type CdTe Electrodes in Acetonitrile/Electrolyte Solutions. Nearly Ideal Behavior from Reductive Surface Pretreatments. *J. Phys. Chem. C* **1983,** *87*, 5140-5150.

(37) Trzhaskovskaya, M. B. Photoelectron Angular Distribution Parameters for Elements Z= 1 to Z=54 in the Photoelectron Energy Range 100-5000eV. *At. Data Nucl. Data Tables* **2001,** *77*, 97-159.
(38) Pookpanratana, S.; Repins, I.; Bär, M.; Weinhardt, L.; Zhang, Y.; Félix, R.; Blum, M.; Yang, W.; Heske C. CdS/Cu(In,Ga)Se_2 Interface Formation in High-Efficiency Thin Film Solar Cells. *Appl. Phys. Lett.* **2010,** *97*, 074101.
(39) Bär, M.; Repins, I.; Weinhardt, L.; Alsmeier, J.-H.; Pookpanratana, S.; Blum, M.; Yang, W.; Heske, C.; Wilks, R. G.; Nouf, R. Zn−Se−Cd−S Interlayer Formation at the CdS/$Cu_2ZnSnSe_4$ Thin-Film Solar Cell Interface. *ACS Energy Lett.* **2017,** *2*, 1632-1640.